Composite Structures 211 (2019) 318–336

Contents lists available at ScienceDirect

Composite Structures

journal homepage: www.elsevier.com/locate/compstruct

Effect of wall thickness and cutting parameters on drilling of glass microballoon/epoxy syntactic foam composites

H.S. Ashrith[a], Mrityunjay Doddamani[a,*], Vinayak Gaitonde[b]

[a] Lightweight Materials Laboratory, Department of Mechanical Engineering, National Institute of Technology Karnataka, Surathkal, India
[b] Department of Industrial and Production Engineering, BVB College of Engineering and Technology, Hubli, Karnataka, India

ARTICLE INFO

Keywords:
Syntactic foam
Drilling
GMB wall thickness
Response surface methodology
Grey relation analysis

ABSTRACT

Effect of glass microballoon (GMB) wall thickness and cutting parameters (cutting speed, feed and drill diameter) on thrust force (F_t), surface roughness (R_a), specific cutting coefficient (K_f), cylindricity (*CYL*), circularity error ($C_{e\text{-}Exit}$) and damage factor ($F_{d\text{-}Exit}$) in drilling of GMB/epoxy syntactic foam is presented. CNC vertical machining centre is utilised for conducting experiments based on full factorial design. Significant process parameters are identified through response surface methodology. Wall thickness significantly affects the $C_{e\text{-}Exit}$ and *CYL* of the drilled hole. Increasing wall thickness significantly reduces the R_a (30%), *CYL* (41%) and $C_{e\text{-}Exit}$ (56%) due to the increased thermal stability of syntactic foams. This observation is very crucial for the syntactic foams used in structural applications pertaining to structural stability. Drill diameter is observed to be significant for F_t, R_a, *CYL* and $F_{d\text{-}Exit}$; while K_f is governed by feed. Furthermore, grey relation analysis (GRA) is used to identify the specific combination of process parameters to obtain good quality drilled hole. Combination of higher particle wall thickness and feed, lower cutting speed and drill diameter produces a sound hole quality as observed from GRA. Hole quality is highly influenced by drill diameter followed by cutting speed and GMB wall thickness. The present study offers guidelines for the industries (structural applications) to produce quality holes in GMB reinforced epoxy matrix.

1. Introduction

Syntactic foams (SFs) are a special class of particulate composites developed by incorporating the rigid hollow particles in a matrix medium [1–3]. Syntactic foams are most commonly used in various marine, aerospace, automobile and civil structural applications owing to their low density combined with excellent compressive properties and low moisture absorption. These closed cell foams are also used in electronic packaging and insulation due to high thermal stability [3]. Hollow particles (also called microballoons) of glass, metal, polymers, carbon, ceramics and fly ash cenospheres have been used in SF fabrication [4–12]. Among different available hollow particles, glass microballoons (GMBs) are the most commonly used as compared to naturally available cenospheres due to better surface morphology [4]. Incorporation of these GMBs offers a wide range of properties to SFs like reduced density, improved impact strength, thermal and dimensional stability [13].

Epoxy resin with GMBs as fillers are extensively investigated for compressive, tensile, flexural, electrical and thermal properties in the recent past [14–21]. Studies on the compressive properties reveal that the strength increases with density. Variation of filler content is not having any significant effect on the compression strength of the syntactic foam. Compressive modulus of syntactic foam depends on the GMBs wall thickness and found to be increasing with increasing content of thick-walled particles [14–17]. Tensile test of syntactic foams reveals that the modulus and strength are found to be increasing with decreasing microballoon content. Modulus and strength can be improved by using thick-walled hollow particles [14,18,19]. Thermal studies reveal that incorporation of GMBs in epoxy helps to reduce the coefficient of thermal expansion and increases dimensional stability. It is also found that the dimensional stability of syntactic foam can be increased by increasing the wall thickness of GMBs [20,21].

Structural components in weight sensitive applications of aerospace and automobile industries demand assembly of syntactic foams

Abbreviations: ANOVA, analysis of variance; CFRP, carbon fiber reinforced polymer; CNC, computer numerical control; CTE, coefficient of thermal expansion; FFD, full factorial design; GFRP, glass fiber reinforced polymer; GMB, glass microballoon; GRA, grey relation analysis; MWCNT, multi-walled carbon nanotube; RSM, response surface methodology; SF, syntactic foam; TiAlN, titanium aluminium nitride

* Corresponding author.
E-mail address: mrdoddamani@nitk.edu.in (M. Doddamani).

https://doi.org/10.1016/j.compstruct.2018.12.022
Received 16 August 2018; Received in revised form 6 November 2018; Accepted 11 December 2018
Available online 17 December 2018

Nomenclature

$C_{e\text{-}Exit}$	exit side circularity error (mm)
CYL	cylindricity (mm)
D	drill diameter (mm)
D_{max}	max. dia. of damage zone (mm)
f	feed (mm/rev)
$F_{d\text{-}Exit}$	exit side damage factor
F_t	thrust force (N)
K_f	specific cutting coefficient (MPa)
m	experiments
n	parameters
R_a	surface roughness (μm)
v	cutting speed (m/min)
w	wall thickness of GMB (μm)
$Y_e^o(p)$	original data sequence
$Y_e^*(p)$	pre-processed data sequence
γ_e	grey relation grade
Φ_v	matrix porosity (vol%)
ρ_e	experimental density (kg/m^3)
ρ_t	theoretical density (kg/m^3)
$\xi_e(p)$	grey relation coefficient
ζ	identification coefficient

requiring drilling operation. However, syntactic foams drilling is quite challenging as drill experiences variable resistance while passing through the matrix, wall thickness of GMB and void space within GMB. Such variations in resistance might affect drilled hole quality significantly and hence needs to be addressed. Further, abrasive nature of GMBs may result in tool wear which significantly deteriorates the hole quality. Hence, the drilling behavior of syntactic foams needs to be thoroughly studied particularly in case of GMB wall thickness variations.

A number of research publications for evaluating the drilling behavior of polymer composites have been published. El-Sonbaty et al. [22] analysed the effects of cutting and work material parameters on torque, thrust force and roughness in glass fiber reinforced polymer (GFRP) drilling using high-speed steel twist drills. Gaitonde et al. [23] established the relation between speed and feed with surface roughness in high-speed drilling of polyamides using response surface methodology (RSM). For the same polyamide material, Rubio et al. [24] used Taguchi method to analyse the effects of tool geometry and cutting parameters on thrust force, circularity error and hole diameter. Liu et al. [25] optimized the cutting parameters in machining of titanium alloy under minimum quantity lubrication condition using a new flexible method called coupling response surface methodology. Results show that surface roughness and cutting forces can be minimized by adopting lower values of feed and depth of cut. Taguchi method coupled with GRA has been used by Palanikumar et al. [26] to optimize the process parameters for minimizing the surface roughness and thrust force in GFRP composite drilling. The effect of multi-walled carbon nanotube (MWCNT) in laser drilling of MWCNT reinforced GFRP nanocomposite composites has been reported by Palanikumar [27]. Results show that the addition of MWCNT significantly improves the hole quality due to enhanced heat transfer characteristics of the composite. Basavarajappa et al. [28] proposed RSM based mathematical expressions to correlate v and f with F_t, R_a and K_f for GFRP composites drilling.

Krishnaraj et. al. [29] conducted high-speed drilling of carbon fiber reinforced polymer (CFRP) laminates to analyse process parameters influence on thrust force, circularity, delamination, and hole size. Furthermore, multi-response optimization has been performed to improve the quality of drilled holes [30]. The effect of cutting speed and feed on drilling forces, burrs, hole wall surface morphology and delamination damage in drilling of high-strength T800S/250F CFRP laminate has been analysed by Xu et al. [31] using coated twist and dagger drill. Xu et al. [32] proposed evaluation criteria for quantifying the defects induced during drilling of T800/X850 CFRP laminates using three different types of drills. The effect of different cutting sequence, tool geometry and tool materials in drilling of hybrid CFRP/Titanium stacks have been studied by Xu and El Mansori [33]. Results reveal that the drill geometry significantly effects drilling of CFRP/Titanium stacks than tool material composition. Drilling from titanium to CFRP phase produces sound quality holes in terms of consistent hole diameters and better surface finish. Ameur et al. [34] analysed the effect of process parameters on cylindricity error and delamination in dry drilling of CFRP composites. Saoudi, Zitoune [35] proposed a unique analytical model for predicting critical thrust force responsible for delamination considering the effect of the chisel and cutting edges in drilling of CFRP composites. Effect of cutting speed and feed on the temperature generated during drilling of CFRP and GFRP composites has been reported by Sorrentino, Turchetta [36]. Finally, a numerical model has been proposed based on experimental data for predicting the temperature generated during drilling of composites. An effort has been made by Merino-Perez et al. [37] to study the effect f, v and workpiece constituents in CFRP composites drilling.

Despite the availability of exhaustive literature on drilling of polymer composites, studies influence of wall thickness variations (different density particles) on epoxy based syntactic foams is not yet reported. Thereby in the present investigation, an effort has been made to analyse the drilling behavior of GMB/epoxy syntactic foam with particle wall thickness variation. Influence of process parameters (v, f, w and D) on responses such as F_t, R_a, K_f, CYL, $C_{e\text{-}Exit}$ and $F_{d\text{-}Exit}$ are presented. Furthermore, based on the experimental analysis, grey relation optimization is performed to propose a specific combination of process parameters to achieve better machinability and hole quality which might act as a guideline in industrial practices.

2. Materials and methods

2.1. Constituent materials

Syntactic foams specimens are fabricated using GMBs reinforced in

Table 1
Density and porosity values of fabricated syntactic foams.

GMB type	w	SF type	ρ_t	ρ_e	Φ_v	Weight saving potential (%) as compared to neat epoxy
SID-200Z	0.716	E200	596.80	566.3 ± 13.12	5.11	52.49
SID-270Z	0.925	E270	638.80	586.22 ± 10.14	8.23	50.82
SID-350Z	1.080	E350	686.80	625.26 ± 12.45	8.96	47.55

Table 2
Drilling process parameters [21,22,27,39–41].

Parameters	# Levels	Levels		
v	3	25	75	125
f	3	0.04	0.08	0.12
D	3	8	12	16
w	3	0.716	0.925	1.080
Replications	3			

LAPOX (L-12) epoxy resin with K-6 polyamine hardener procured from Atul Ltd., Valsad, India. Epoxy matrix is reinforced with three different density grades (particle wall thickness variations) of hollow borosilicate GMBs (SID-200Z, SID-270Z and SID-350Z) procured from Trelleborg Offshore, USA. Wall thickness, density and mean particle size of SID-200Z, SID-270Z and SID-350Z grade hollow particles are 0.716, 0.925, 1.080 μm; 200, 270, 350 kg/m^3 and 53, 50, 45 μm respectively. GMBs are used without any surface treatment.

2.2. Syntactic foam fabrication

Syntactic foams of three different types are fabricated using three grades of GMBs having varying wall thickness with 60 vol%. Volume fraction of GMB is fixed based on the earlier investigation [38]. SFs are fabricated using a two-step process. Initially, a weighed quantity (60 vol %) of GMBs is mixed with epoxy resin manually by slow stirring to form a homogenous mixture. In the second step, 10 wt% of hardener is added to mixture and stirred for an additional five minutes. The mixture is degassed prior to pouring into the molds of dimension Ø35 × 16 mm. For easy removal of the cast specimens, interior mold surface is smeared with silicone releasing agent. Specimens are cured for 24 h at room temperature followed by 2 h of post-curing at 90 °C. In total 81 specimens are fabricated for each particle wall thickness variation. All samples are coded as EYYY wherein 'E' represents epoxy resin while 'YYY' signifies the true particle density of GMBs. For example, "E350" syntactic foam indicates 350 kg/m^3 density GMBs (1.080 μm wall thickness) are dispersed in epoxy resin.

2.3. Density measurement

ASTM standard C271-16 is used for density estimation of all the specimens. Neat epoxy density (1192 kg/m^3) is used in the rule of mixtures for calculating the syntactic foams theoretical density [19]. Weight saving potential of the foams is also computed and are presented in Table 1.

2.4. Planning of experiments

Many parameters affect the quality of drilled holes, among them cutting speed, feed and drill diameter are found to be the significant parameters [27] and hence are considered as input process parameters in the present work along with GMB wall thickness. F_t, R_a, K_f, CYL, $C_{e\text{-}Exit}$ and $F_{d\text{-}Exit}$ are identified as the responses. Process parameter and their levels are selected based on the earlier investigations [21,22,27,38–41]. From the literature survey, it is observed that the cutting speed in the range of 20–200 m/min and feed in the range of 0.03–0.5 mm/rev is typically employed in drilling of polymer composites [39,42]. Also, using high cutting speed results in higher cutting temperature which may reduce the drill life. GMBs wall thickness is chosen based on high collapse strength exhibited by the hollow particles and the drill diameters are selected to suit the application requirements of syntactic foams. Based on this criterion, the process parameters and their levels presented in Table 2 are considered for conducting the drilling experiments. From authors earlier investigations, it is observed that increasing GMBs content significantly improves the hole quality. Thereby, GMBs content is fixed at 60 vol%

Table 3
Experimental layout plan and the measured average value of responses.

w	v	f	D	F_t[a]	R_a[a]	K_f[a]	CYL[a]	$C_{e\text{-}Exit}$[a]	$F_{d\text{-}Exit}$[a]
0.716	25	0.04	8	19.62	4.12	122.63	0.022	0.024	1.003
			12	39.24	2.81	163.50	0.024	0.030	1.004
			16	58.86	2.11	183.94	0.030	0.044	1.007
		0.08	8	29.43	3.20	91.97	0.024	0.019	1.003
			12	49.05	2.20	102.19	0.030	0.030	1.005
			16	78.48	1.97	122.63	0.035	0.042	1.007
		0.12	8	39.24	3.12	81.75	0.031	0.016	1.004
			12	68.67	2.19	95.38	0.032	0.021	1.005
			16	98.10	1.29	102.19	0.043	0.031	1.008
	75	0.04	8	19.62	4.12	122.63	0.022	0.028	1.001
			12	29.43	3.11	122.63	0.027	0.036	1.004
			16	49.05	2.16	153.28	0.037	0.056	1.006
		0.08	8	29.43	3.39	91.97	0.025	0.026	1.003
			12	49.05	2.88	102.19	0.034	0.034	1.005
			16	68.67	2.32	107.30	0.040	0.044	1.007
		0.12	8	29.43	3.15	61.31	0.031	0.018	1.003
			12	58.86	2.77	81.75	0.035	0.026	1.005
			16	88.29	1.63	91.97	0.048	0.040	1.008
	125	0.04	8	19.62	4.25	122.63	0.024	0.030	1.001
			12	29.43	3.32	122.63	0.031	0.044	1.003
			16	39.24	2.99	122.63	0.041	0.060	1.005
		0.08	8	19.62	3.99	61.31	0.025	0.026	1.002
			12	39.24	3.19	81.75	0.034	0.040	1.004
			16	58.86	2.56	91.97	0.042	0.047	1.005
		0.12	8	29.43	3.73	61.31	0.032	0.019	1.003
			12	49.05	2.66	68.13	0.040	0.031	1.003
			16	68.67	2.20	71.53	0.055	0.042	1.007
0.925	25	0.04	8	29.43	3.03	183.94	0.010	0.013	1.003
			12	49.05	2.54	204.38	0.014	0.025	1.005
			16	58.86	1.08	183.94	0.027	0.026	1.007
		0.08	8	39.24	2.94	122.63	0.014	0.007	1.004
			12	68.67	1.26	143.06	0.023	0.010	1.006
			16	88.29	1.08	137.95	0.030	0.020	1.008
		0.12	8	39.24	2.06	81.75	0.020	0.004	1.004
			12	68.67	1.14	95.38	0.026	0.009	1.006
			16	107.91	1.07	112.41	0.041	0.015	1.008
	75	0.04	8	29.43	3.26	183.94	0.014	0.017	1.003
			12	39.24	2.75	163.50	0.019	0.028	1.004
			16	58.86	2.03	183.94	0.028	0.036	1.007
		0.08	8	39.24	3.09	122.63	0.016	0.011	1.003
			12	58.86	2.43	122.63	0.026	0.016	1.005
			16	78.48	1.95	122.63	0.037	0.031	1.007
		0.12	8	39.24	2.54	81.75	0.022	0.009	1.004
			12	58.86	2.20	81.75	0.033	0.014	1.006
			16	98.10	1.52	102.19	0.041	0.019	1.008
	125	0.04	8	19.62	4.76	122.63	0.017	0.021	1.002
			12	39.24	3.00	163.50	0.025	0.028	1.004
			16	58.86	2.64	183.94	0.033	0.055	1.006
		0.08	8	29.43	3.84	91.97	0.018	0.013	1.003
			12	58.86	2.68	122.63	0.030	0.023	1.005
			16	78.48	2.15	122.63	0.041	0.034	1.007
		0.12	8	39.24	3.79	81.75	0.026	0.011	1.003
			12	58.86	2.68	81.75	0.033	0.020	1.005
			16	98.10	1.55	102.19	0.045	0.030	1.008
1.080	25	0.04	8	29.43	2.78	183.94	0.010	0.006	1.003
			12	49.05	0.87	204.38	0.012	0.009	1.006
			16	78.48	2.10	245.25	0.022	0.023	1.007
		0.08	8	39.24	2.22	122.63	0.014	0.004	1.004
			12	58.86	0.79	122.63	0.018	0.007	1.006
			16	98.10	1.15	153.28	0.028	0.013	1.008
		0.12	8	39.24	1.92	81.75	0.015	0.003	1.005
			12	68.67	1.00	95.38	0.023	0.005	1.007
			16	98.10	1.11	102.19	0.036	0.011	1.009
	75	0.04	8	29.43	2.96	183.94	0.007	0.010	1.003
			12	39.24	1.78	163.50	0.012	0.014	1.006
			16	68.67	2.65	214.59	0.020	0.026	1.007
		0.08	8	39.24	3.00	122.63	0.010	0.009	1.004
			12	68.67	1.55	143.06	0.014	0.011	1.007
			16	107.91	1.72	168.61	0.027	0.026	1.008
		0.12	8	49.05	2.39	102.19	0.014	0.007	1.004
			12	68.67	1.44	95.38	0.015	0.010	1.007
			16	117.72	2.56	122.63	0.029	0.017	1.009

(*continued on next page*)

Table 3 (*continued*)

w	v	f	D	F_t[a]	R_a[a]	K_f[a]	CYL[a]	$C_{e\text{-}Exit}$[a]	$F_{d\text{-}Exit}$[a]
	125	0.04	8	19.62	3.58	122.63	0.013	0.014	1.004
			12	49.05	1.33	204.38	0.018	0.022	1.006
			16	78.48	1.90	245.25	0.024	0.037	1.008
		0.08	8	39.24	4.75	122.63	0.016	0.010	1.005
			12	68.67	1.66	143.06	0.019	0.017	1.007
			16	107.91	1.42	168.61	0.031	0.031	1.008
		0.12	8	49.05	3.68	102.19	0.016	0.010	1.006
			12	78.48	1.00	109.00	0.024	0.017	1.008
			16	117.72	1.26	122.63	0.037	0.029	1.009

[a] Average of 3 tests.

[38]. Three levels for each input process parameters are selected (Table 2) to consider the nonlinear effects among the parameters. Table 3 presents the experimental layout plan based on full factorial design (FFD) [43] and measured average values (three replicates) of the responses. Standard deviation values are not presented in Table 3, as observed deviations are < 3%.

2.5. Drilling experiments

Drilling investigations are conducted on a vertical computer numerical control (CNC) machining center (MAX MILL PLUS+, MTAB Engineers Pvt. Ltd., India) as per FFD. Three types of syntactic foams (E200, E270 and E350) with varying GMB wall thickness are tested using coated solid tungsten carbide twist drills. Fig. 1 shows the experimental setup used for conducting drilling experiments. Thrust force is measured using a strain gauge type of dynamometer (Syscon Instruments Pvt. Ltd., India). Mitutoyo surftest (SJ 301, Japan) with 0.8 mm cut-off length is used to estimate the surface roughness of the drilled hole. Cylindricity and circularity error of drilled holes are measured using Evolution 20.12.10, METRIS, UK make coordinate measuring machine. Specific cutting coefficient is defined as the ratio of total energy input rate by material removal rate. It is observed to be an important material characteristic and gives a good indication of the machining effort. Specific cutting coefficient is computed using [28],

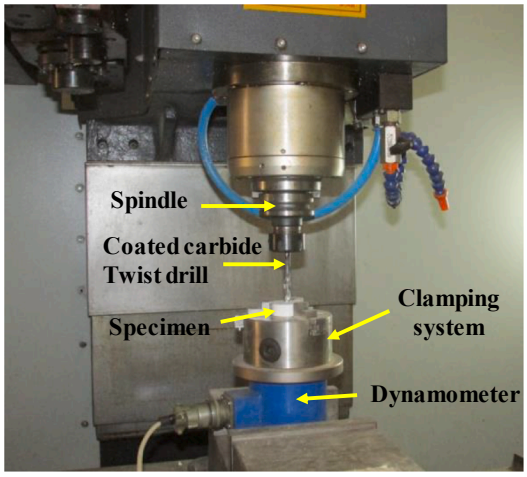

Fig. 1. Experimental setup.

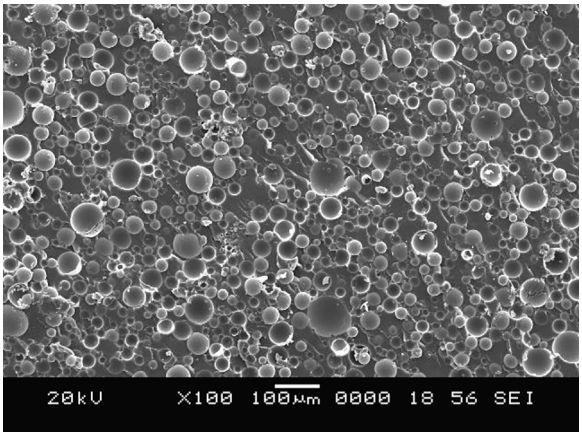

Fig. 2. SEM of representative E200 sample showing uniform distribution of GMBs in epoxy matrix.

$$K_f = \frac{2 \times F_t}{f \times D} \tag{1}$$

Since syntactic foam is a particulate composite (non-laminate), damage factor is considered instead of delamination factor. Drilling-induced damage on the exit side is more severe than on the entry side [31]. Further, the damage observed on the entry side in the present work is found to be very negligible as compared to the exit side damage and hence it is not considered during the present investigation. Damage factor at the hole exit is estimated using most commonly used approach and is given by [44,45],

$$F_{d-Exit} = \frac{D_{\max}}{D} \tag{2}$$

Input parameters (I) and their respective levels (L) are coded as I_L. For example, $f_{0.04}$ denotes feed of 0.04 mm/rev. Experimentally measured average values are presented in Table 3.

2.6. Response surface methodology

Conventional method requires a large number of experiments to be carried out and is generally time consuming [46]. Also, the conventional method does not consider the interaction effects among the various input process parameters. RSM is a group of mathematical and statistical techniques which are useful for developing mathematical models based on FFD to analyse a response influenced by several input parameters [47]. It has been widely used to study the drilling behavior [23,47,48]. RSM based mathematical expressions are proposed using the experimental results presented in Table 3. RSM based models provide necessary information about the main and interaction effect of input parameters on the responses with a limited number of experiments [47]. The general representation of RSM based model can be written as [43],

$$Y = \varphi(x_1, x_2, x_3, \ldots\ldots, x_k) \tag{3}$$

where Y is response, $x_1, x_2, x_3, \ldots\ldots x_k$ are input variables and φ is response function. Generally, a second order mathematical model is generated in RSM [34] to find the relationship between the response and input process parameters which is given by,

$$Y = \begin{pmatrix} a_0 + a_1 \times v + a_2 \times f + a_3 \times D + a_4 \times R + a_{11} \times v^2 + a_{22} \times f^2 \\ \quad + a_{33} \times D^2 + a_{44} \times R^2 + a_{12} \\ \times v \times f + a_{13} \times v \times D + a_{14} \times v \times R + a_{23} \times f \times D + a_{24} \times f \times R \\ \quad + a_{34} \times D \times R \end{pmatrix} \tag{4}$$

where $a_0, a_1, \ldots a_{34}$ are the regression coefficients of the model. Based on the experimental data as presented in Table 3, RSM models are developed for analysis and interpretation.

2.7. Grey relation optimization

RSM is widely used for single response optimization. Optimization based on RSM may result in different optimum conditions for multiple

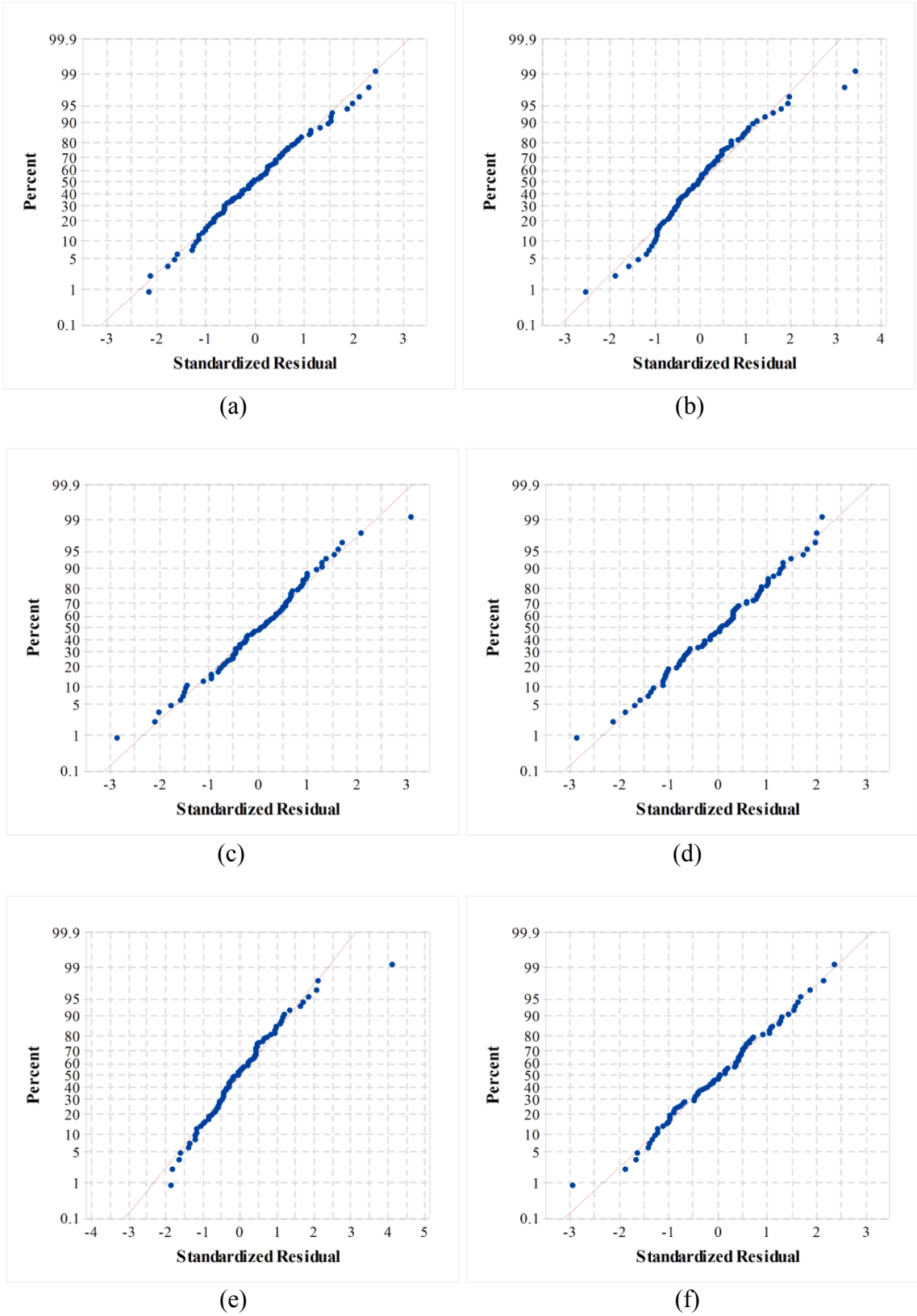

Fig. 3. Normal probability plots for (a) F_t (b) R_a (c) K_f (d) CYL (e)C_{e-Exit} and (f) F_{d-Exit}.

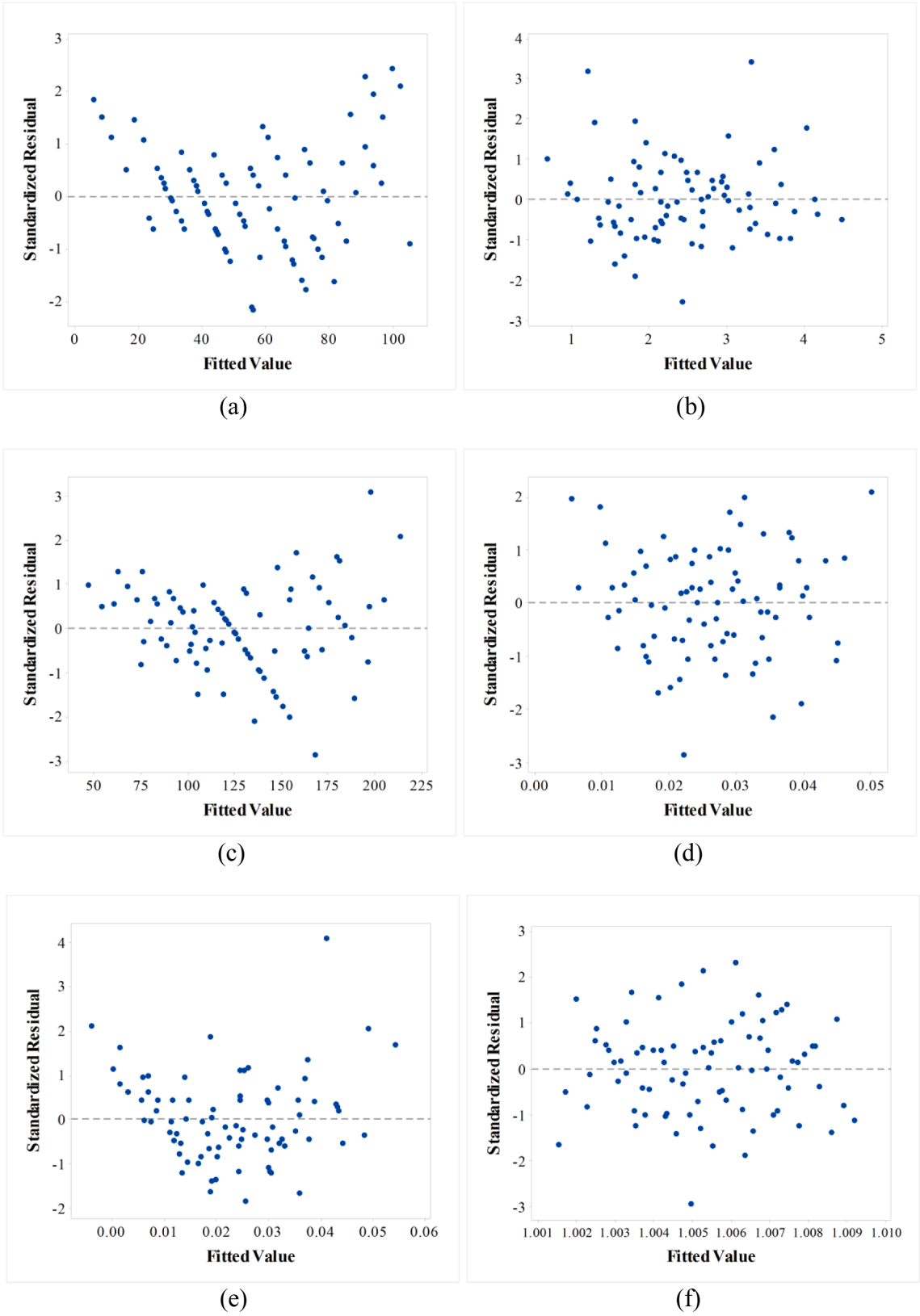

Fig. 4. Residual fit plots for (a) F_t (b) R_a (c) K_f (d) CYL (e)C_{e-Exit} and (f) F_{d-Exit}.

Table 4
Summary of ANOVA results for the developed mathematical models.

Responses	Sum of squares		Degrees of freedom		Mean square		F-ratio	P-Value	R^2
	Regression	Residual	Regression	Residual	Regression	Residual			
F_t	5.02×10^4	1.77×10^3	14	66	3.59×10^3	26.83	133.78[a]	< 0.001	0.9660
R_a	59.09	13.45			4.22	0.20	20.71[a]	< 0.001	0.8145
K_f	1.33×10^5	1.16×10^4			9.53×10^3	175	54.43[a]	< 0.001	0.9203
CYL	7.96×10^{-3}	3.61×10^{-4}			5.68×10^{-4}	5.00×10^{-6}	103.92[a]	< 0.001	0.9566
C_{e-Exit}	1.33×10^{-2}	4.57×10^{-4}			9.48×10^{-4}	7.00×10^{-6}	137.10[a]	< 0.001	0.9668
F_{d-Exit}	3.02×10^{-4}	9.00×10^{-6}			2.20×10^{-5}	1.41×10^{-7}	156.50[a]	< 0.001	0.9708

Significance at 99 % confidence interval.
[a] F-table = 2.36.

responses. Optimum condition of a specific response may be detrimental for other responses. Hence, multi-objective optimization needs to be performed for simultaneous optimization of multiple responses. Therefore, present work deals with GRA to obtain optimum process parameter settings by converting multiple responses into a single normalized response. The different steps involved in GRA are,

1. Normalizing the experimental data using lower-the-better scheme of GRA.
2. Identifying the grey relation coefficients using the normalized data.
3. Computing the grey relation grade by averaging grey relation coefficients.

Finally, optimization value is presented for minimizing the chosen responses which results in best hole quality. This data is very useful for industry practitioners for achieving the structural stability of the foam components.

2.8. Imaging

Scanning electron microscopy is conducted using JSM 6380LA, JEOL, Japan. Gold is used for sputter coating of all the samples (JFC-1600, JEOL, Japan) prior to imaging.

3. Result and discussion

3.1. Syntactic foam microstructure and density

Extensive micrography is conducted on the as-cast syntactic foam samples. Fig. 2 shows a representative micrograph of as cast syntactic foam sample. Microballoons are observed to be uniformly distributed throughout the epoxy matrix without forming the clusters. Particle debris is not seen in the epoxy matrix indicating intact particles during processing. During syntactic foam fabrication air is entrapped in the matrix resin leading to matrix porosity. Densities of syntactic foams along with matrix porosity is presented in Table 1. Experimental density is found to be lesser than the theoretical density of syntactic foams indicating the presence of hollow microballoons and air entrapment in the matrix resin. Thick-walled GMBs being stiffer requires more force to disperse them in the matrix leading to increased air entrapment, which subsequently increases matrix porosity. It is also found that the density of the syntactic foams increases with increasing GMBs wall thickness. Compared to neat epoxy, density reduction is in the range of 48–53% indicating significant weight saving potential.

3.2. Development of mathematical models

Mathematical models for the considered responses (F_t, R_a, K_f, CYL, $C_{e\text{-}Exit}$ and $F_{d\text{-}Exit}$) are developed using the experimental data presented in Table 3. Since the process parameters (w, v, f and D) are considered at multi-levels, second-order mathematical models based on RSM are proposed for predicting the responses within the chosen range of process parameters. Regression equations for the different responses are developed using commercially available Minitab version 14 software and are given as,

$$F_t = \begin{pmatrix} 77.73 - 94.32 \times w - 0.53 \times v + 226.59 \times f - 6.45 \times D + 14.39 \times w^2 \\ - 0.0001 \times v^2 - 2611.46 \\ \times f^2 + 0.18 \times D^2 + 0.53 \times w \times v + 70.64 \times w \times f + 6.19 \times w \times D \\ + 0.27 \times v \times f - 0.003 \times v \times D \\ + 35.77 \times f \times D \end{pmatrix} \quad (5)$$

$$R_a = \begin{pmatrix} 11.35 - 2.87 \times w + 0.02 \times v - 21.51 \times f - 0.92 \times D - 0.85 \times w^2 \\ - 3.73 \times 10^{-5} \times v^2 - 11.00\times \\ f^2 + 0.03 \times D^2 + 0.004 \times w \times v + 9.64 \times w \times f + 0.09 \times w \times D \\ + 0.02 \times v \times f - 0.001 \times v \times D \\ + 0.17 \times f \times D \end{pmatrix} \quad (6)$$

$$K_f = \begin{pmatrix} 119.09 + 142.91 \times w - 1.33 \times v - 830.49 \times f - 2.10 \times D \\ - 34.7 \times w^2 - 0.0002 \times v^2 + 6820.41 \\ \times f^2 + 0.09 \times D^2 + 0.86 \times w \times v - 1215.09 \times w \times f \\ + 5.88 \times w \times D + 3.03 \times v \times f + 0.01 \times v \times D \\ - 30.16 \times f \times D \end{pmatrix} \quad (7)$$

$$CYL = \begin{pmatrix} 0.02 + 0.03 \times w + 1.28 \times 10^{-5} \times v + 0.05 \times f - 0.002 \times D \\ - 0.03 \times w^2 + 5.78 \times 10^{-7} \times v^2 + 0.278 \\ \times f^2 + 0.0001 \times D^2 - 0.0001 \times w \times v - 0.06 \times w \times f \\ + 0.0003 \times w \times D - 0.0002 \times v \times f + 4.17 \\ \times 10^{-6} \times v \times D + 0.01 \times f \times D \end{pmatrix} \quad (8)$$

$$C_{e-Exit} = \begin{pmatrix} 0.12 - 0.19 \times w - 0.0001 \times v - 0.24 \times f + 0.001 \times D \\ + 0.08 \times w^2 - 7.41 \times 10^{-8} \times v^2 + 0.51 \\ \times f^2 + 0.0001 \times D^2 + 0.0001 \times w \times v + 0.20 \times w \times f \\ - 0.002 \times w \times D - 0.0002 \times v \times f + \\ 1.14 \times 10^{-5} \times v \times D - 0.01 \times f \times D \end{pmatrix} \quad (9)$$

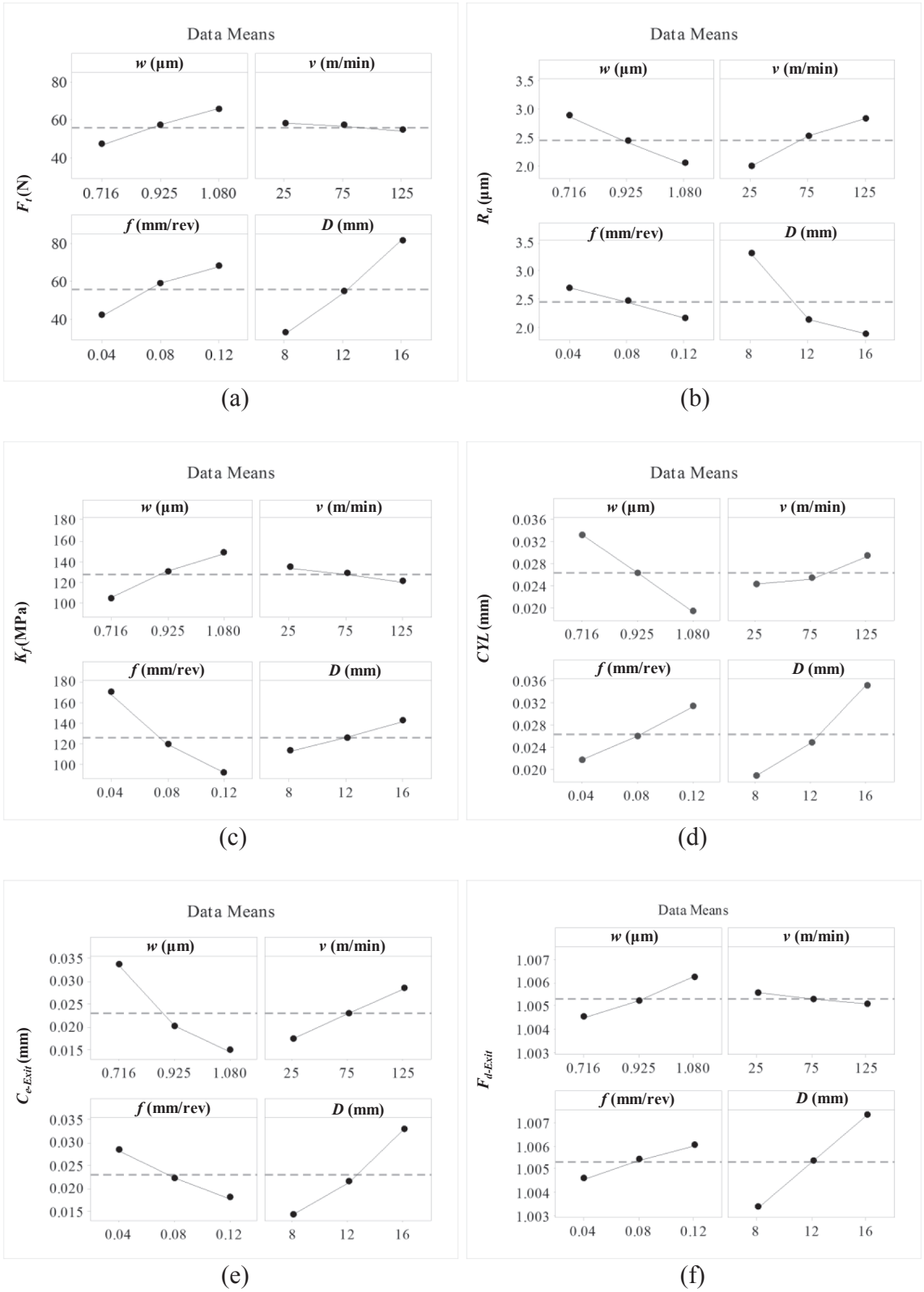

Fig. 5. Main effects plot for (a) F_t (b) R_a (c) K_f (d) CYL (e)C_{e-Exit} and (f) F_{d-Exit}.

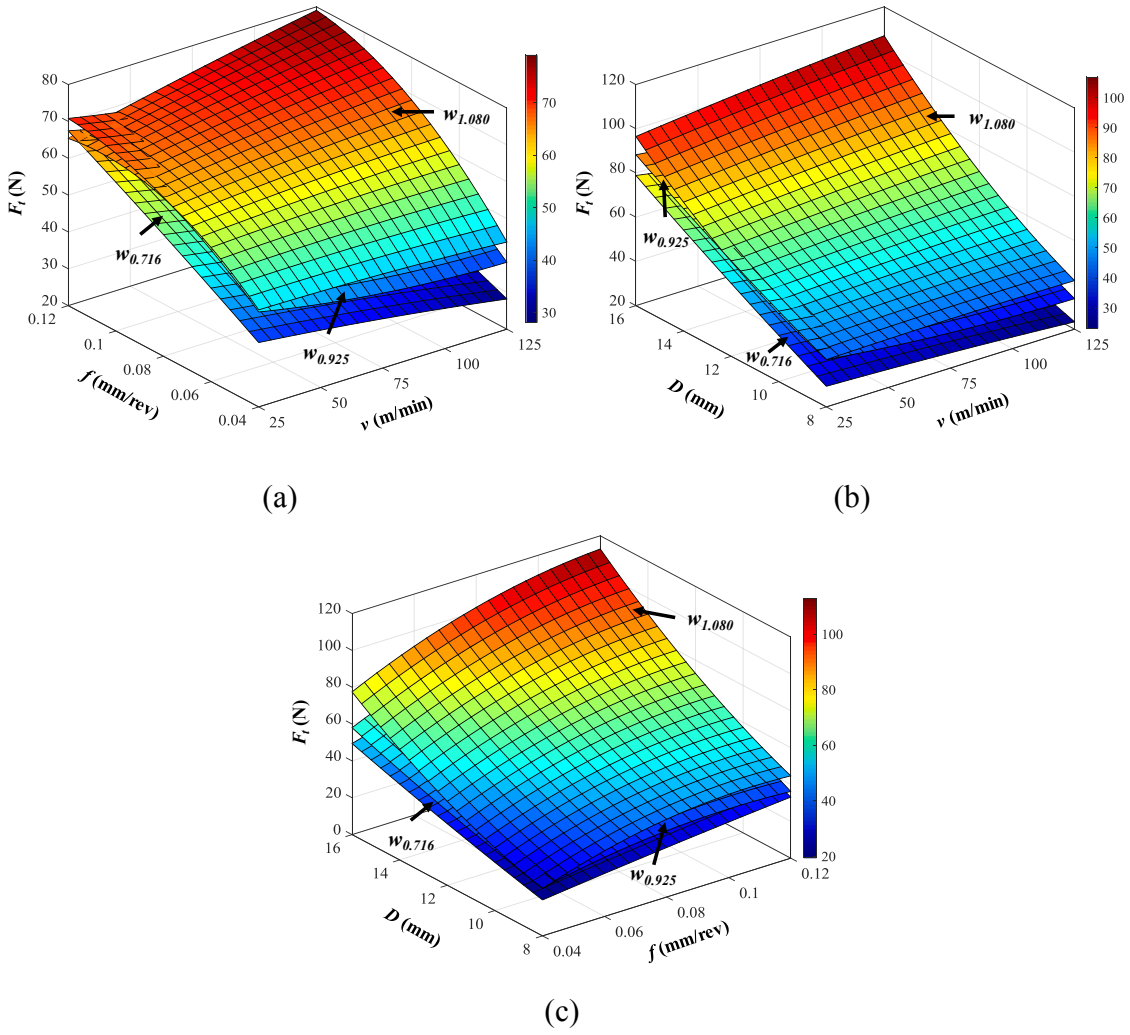

Fig. 6. Response surface plots of (a) v-f, (b) v-D and (c) f-D on Ft for varying wall thickness.

$$F_{d-Exit} = \begin{pmatrix} 1.004 - 0.014 \times w - 0.0001 \times v + 0.032 \times f + 0.0005 \times D \\ + 0.008 \times w^2 - 2.09 \times 10^{-8} \times v^2 \\ - 0.063 \times f^2 + 5.70 \times 10^{-7} \times D^2 + 0.0001 \times w \times v \\ - 0.007 \times w \times f + 2.74 \times 10^{-6} \times w \times D \\ + 2.41 \times 10^{-5} \times v \times f - 2.21 \times 10^{-7} \times v \times D + 0.0001 \times f \times D \end{pmatrix} \quad (10)$$

Eqs. (5)–(10) are used to predict the responses within the chosen range of input process parameters. Normality and homogeneity of the variances are checked before performing ANOVA. Fig. 3 shows the normal probability plots for the responses. It is observed that all the data points are located on the straight-line (except very few) indicating the normal distribution of experimental data. Residual fit plots shown in Fig. 4 are plotted to confirm the goodness-of-fit and homogeneity of the variance in the experimental data. Residual plots (Fig. 4) shows the random distribution of data without any specific pattern indicating the homogeneity of the variances and goodness-of-fit. From both these plots, it is clearly evident that the hypotheses of normality and homogeneity of the residues are validated. Hence, the experimental data can be used for the development of mathematical models. Analysis of variance (ANOVA) is used to validate proposed mathematical expressions adequacy (Table 4). According to ANOVA, the computed F-ratio should be more than the F-table for the models to be adequate. Higher R^2 values indicate the adequacy of developed mathematical models for prediction. The average errors between the experimentally measured and predicted values are found to be 0.74, 4.5, 0.74, 0.95, 0.98 and 0.01% for F_t, R_a, K_f, CYL, $C_{e\text{-}Exit}$ and $F_{d\text{-}Exit}$ respectively indicates a good correlation is existing between the predicted and experimental values. Measurement of surface roughness in reinforced composites is less reliable, because the heterogeneous nature of composite material may lead to large deviations or improper results [49]. Generally, surface roughness of machined surface is considered by averaging the value of several measurements. Deviations among the individual measurements may lead to high error percentage in surface roughness. However, the error between the measured and predicted value falls between 5% and

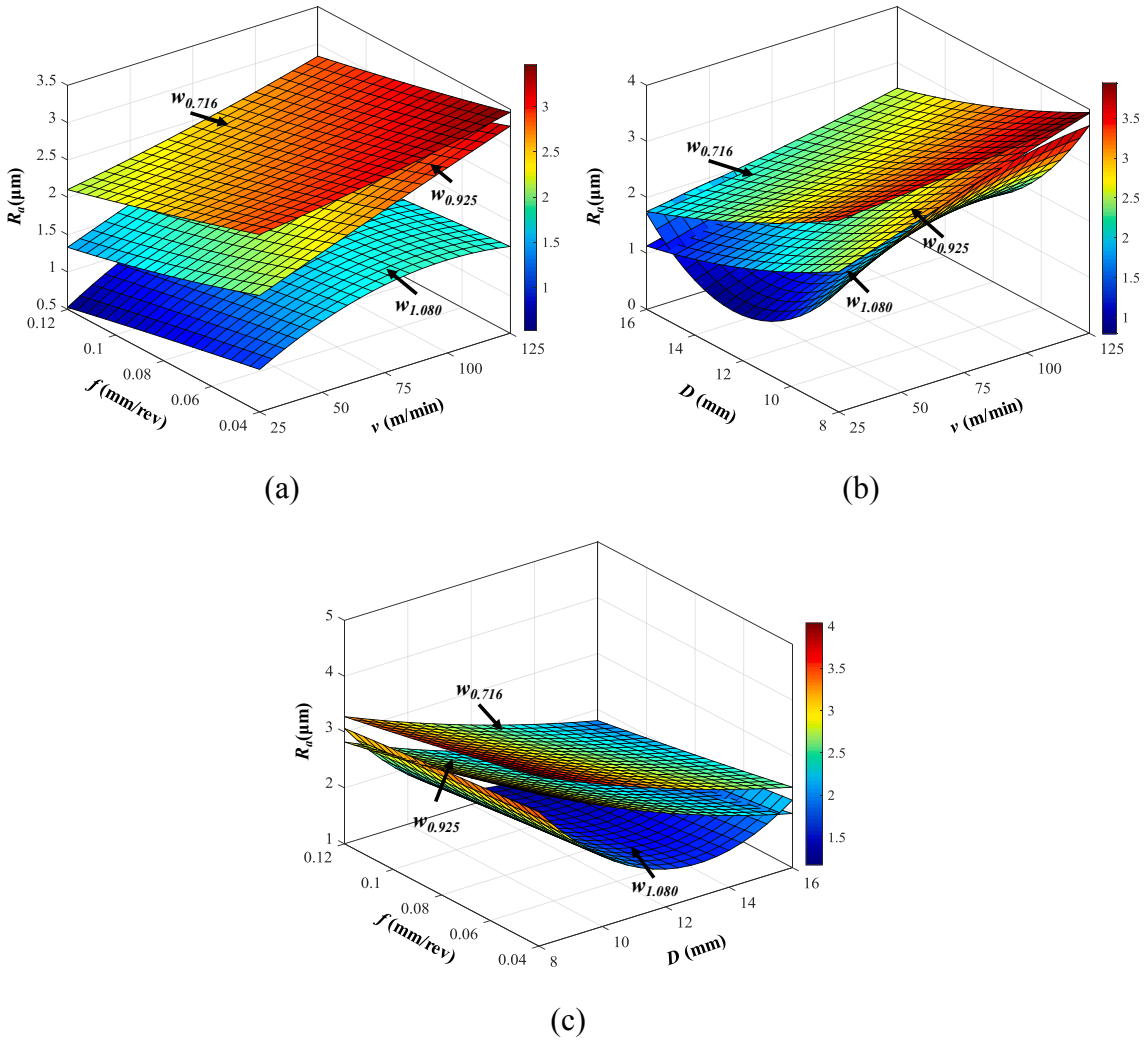

Fig. 7. Response surface plots of (a) v-f, (b) v-D and (c) f-D on Ra for varying wall thickness.

hence the developed mathematical models can be effectively used as a tool in industrial practices to predict the machinability characteristics of varying wall thickness GMB reinforced epoxy foams during drilling.

3.3. Main effects plots

Fig. 5 shows the main effects plots for the responses. F_t increases with increasing w, f, D and slightly decreases with increasing v as seen from Fig. 5a. Fig. 5b shows that R_a increases with increasing v while decreases with increase in w, f and D. K_f increases as w and D increases while it declines with higher values of v and f (Fig. 5c). CYL increases with increasing f, v, D and decreasing w as observed from Fig. 5d. Fig. 5e shows that $C_{e\text{-}Exit}$ increases with D and v while decreasing trend is noted with w and f. Fig. 5f shows increasing w, f, D increases the $F_{d\text{-}Exit}$ while it slightly decreases with increasing cutting speed. These plots are used as a quick reference to understand the general trend between the chosen individual input parameters. Detailed discussion on the observed trends of responses is presented in the following section.

3.4. Response surface plots

Interaction effects among the input process parameters are studied using response surface plots. The plots for varying wall thickness of GMBs are plotted (MATLAB software) using the developed mathematical models (Eqs. (5)–(10)) and are presented in Figs. 6–11.

3.4.1. Thrust force

The variation of F_t with the input parameters such as w, v, f and D are graphed in Fig. 6. F_t increases significantly with the increase in feed. Variation of F_t with increasing cutting speed is found to be very small (Fig. 6a). Increasing feed from $f_{0.04}$ to $f_{0.12}$ increases F_t by 71, 66 and 81% for $w_{0.716}$, $w_{0.925}$ and $w_{1.080}$ respectively. It is known that increasing feed increases the contact area between twist drill and syntactic foam, which in turn increases metal removal rate resulting higher thrust forces [28]. Also, increasing feed increases the cross-sectional area of undeformed chip which in turn increases the resistance for chip formation resulting in higher thrust force [31]. F_t is found to be decreasing with increasing v for $w_{0.716}$ and $w_{0.925}$, while it slightly increases for $w_{1.080}$ (Fig. 6b). Increasing v raises the tool and work

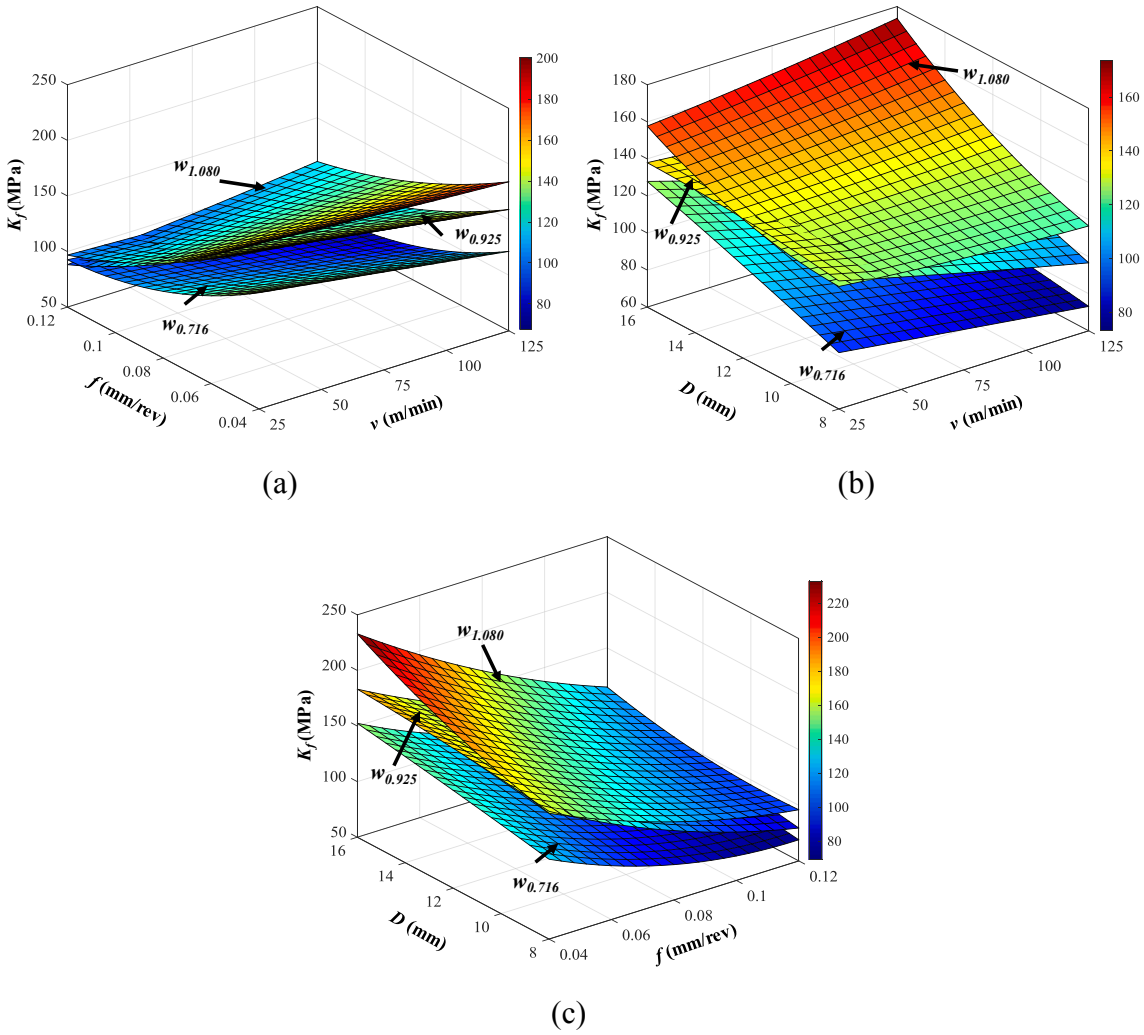

Fig. 8. Response surface plots of (a) v-f, (b) v-D and (c) f-D on Kf for varying wall thickness.

material interface temperature, resulting in the softening of syntactic foam aided by poor thermal conductivity leading to decreased thrust force [34]. It is known that increasing GMB wall thickness increases the compressive strength and decreases the coefficient of thermal expansion (CTE) of syntactic foams, which in turn improves the stiffness of the composite resulting in increased thrust force [21]. F_t increases with D at all the levels of feeds as seen from Fig. 6c. Increasing the drill diameter from D_8 to D_{16}, increases the thrust force by 74, 69 and 46% for $w_{0.716}$, $w_{0.925}$ and $w_{1.080}$ respectively. As drill diameter increases, the contact area of the drilled hole increases leading to higher F_t [22]. It is also noted from Fig. 6 that increasing GMBs wall thickness increases the thrust force. Increasing wall thickness from $w_{0.716}$ to $w_{1.080}$ increases the F_t by 39.84%. This is due to increasing wall thickness of GMBs increases the compressive strength of SFs due to increased collapse strength of GMBs (from 6.9 to 44.8 MPa), which in turn increases cutting resistance of the material for drill advancement resulting in higher thrust forces [14,17,28].

The cutting tools are inspected using a confocal microscope (LEXT, OLS4000, OLYMPUS, Japan) post drilling operation. The tools did not show any signs of tool wear and this may be ascribed to the superior wear resistance of drill due to TiAlN coating. Also, the variation of thrust force with increasing cutting speed is found to be negligible indicating insignificant tool wear. Hence, in the present investigation influence of tool wear on the responses is not considered during the analysis.

3.4.2. Surface roughness

Fig. 7 presents the response surface plots of surface roughness for varying GMB wall thickness. R_a increases with increasing cutting speed and decreasing feed (Fig. 7a). Increasing feed from $f_{0.04}$ to $f_{0.12}$ decreases R_a by 27, 35 and 51% for $w_{0.716}$, $w_{0.925}$ and $w_{1.080}$ respectively. It is known that increasing feed decreases the machining temperature due to the reduced contact time between drill and specimen leading to lower R_a values [22]. Increasing cutting speed increases R_a while decreasing trend is observed with increasing drill diameter except for the SF reinforced with $w_{1.080}$ as observed from Fig. 7b. R_a increases by 15, 56 and 72% for $w_{0.716}$, $w_{0.925}$ and $w_{1.080}$ respectively with increasing cutting speed from v_{25} to v_{125}. Increasing cutting speed increases the temperature at the tool-work material interface aided by the poor thermal conductivity of syntactic foams resulting in rough surface [23].

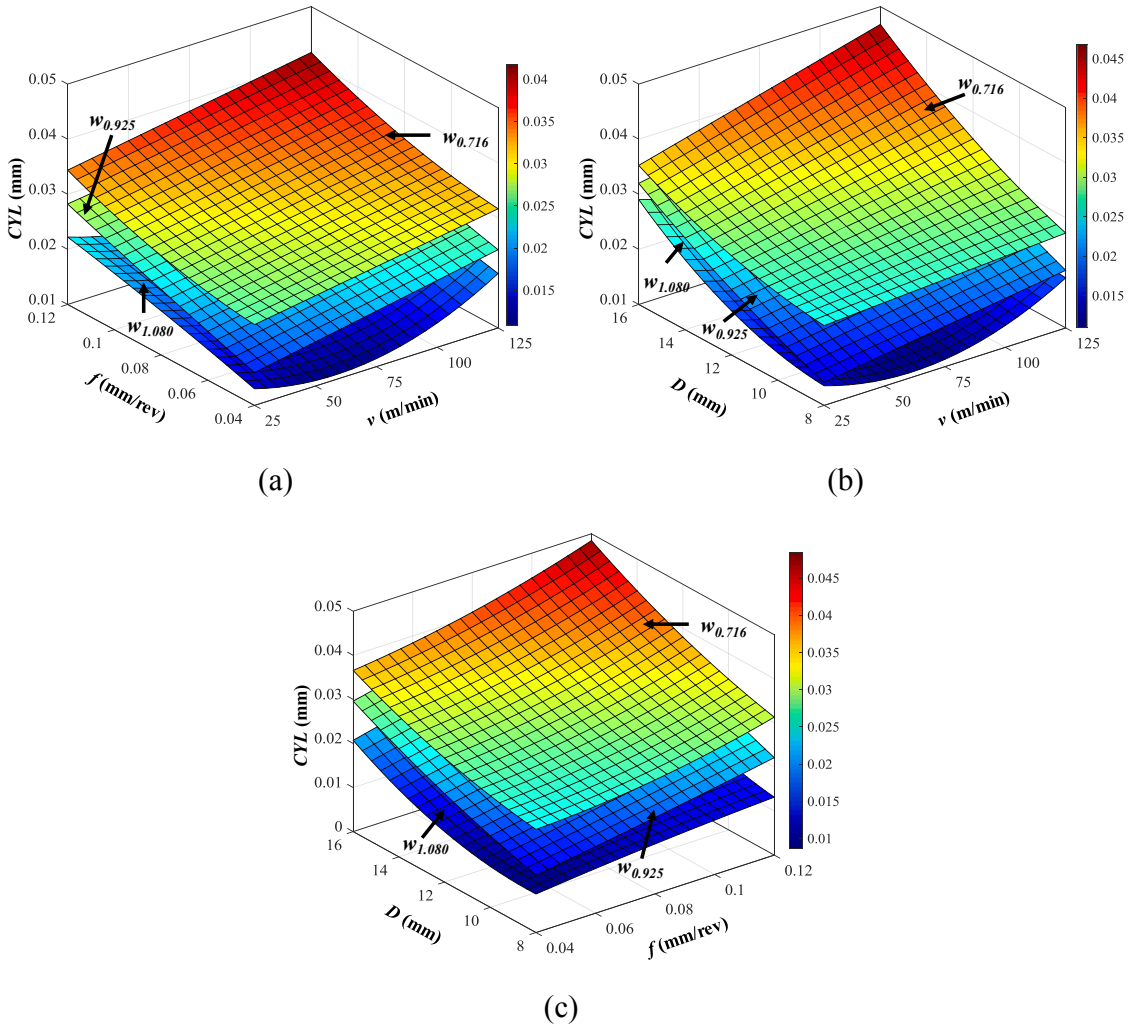

Fig. 9. Response surface plots of (a) v-f, (b) v-D and (c) f-D on CYL for varying wall thickness.

Fig. 7c shows the variation of R_a at different feed and drill diameter. Increasing diameter from D_8 to D_{16} decreases R_a in the range of 35–47% for varying wall thickness. Increasing drill diameter at a given cutting speed reduces the rotational speed of the cutting tool ($N = 1000v/\pi D$). This reduces the rubbing of cutting tool against drilled wall resulting reduced interface temperature, which in turn decreases R_a values [50]. However, the surface roughness is found to be increasing beyond D_{12} for syntactic foam with thick-walled GMB due to higher thrust forces. This may be due to the effect of thrust force being more severe than the effect of decreased interface temperature. SF with thick-walled GMBs ($w_{1.080}$) exhibits lower surface roughness values as compared to thin-walled GMBs ($w_{0.716}$ and $w_{0.925}$) as evident from Fig. 7. Increasing w from $w_{0.716}$ to $w_{1.080}$ decreases R_a by 30% due to the increased thermal stability of syntactic foams with increasing GMBs wall thickness [21]. Further, thick-walled GMBs being stiffer (higher collapse strength), produces an effective burnishing effect than that of thin-walled ones. In case of thick walled GMBs, smearing of the epoxy matrix on drilled surface results in lower roughness values [28].

3.4.3. Specific cutting coefficient

K_f is found to be decreasing with increasing cutting speed and decreasing feed (Fig. 8a). Increasing feed from $f_{0.04}$ to $f_{0.12}$ decreases K_f by 40, 50 and 56% for $w_{0.716}$, $w_{0.925}$ and $w_{1.080}$ respectively. At lower feeds, the shear model could not fit the chip formation process effectively as the syntactic foams is subjected to lower strain rates resulting higher specific cutting coefficient [28]. Fig. 8b shows the variation of K_f with v at different D. K_f decreases by 19 and 25% with the increasing cutting speed for SF with $w_{0.716}$ and $w_{0.925}$, while it increases by 8% for $w_{1.080}$. As explained earlier, increasing cutting speed decreases thrust force in SFs with thin-walled GMBs resulting reduced K_f values, whereas it increases with thick-walled GMB due to increased thrust force with increasing speed. K_f is found to be decreasing with the rise in f and decreasing D (Fig. 8c). Increasing drill diameter from D_8 to D_{16} increases K_f in the range of 11–43% for varying wall thickness. Increasing thrust force with increasing drill diameter leads to higher K_f [51]. Fig. 8 also shows that increasing GMBs wall thickness increases the K_f. Increasing GMBs wall thickness from $w_{0.716}$ to $w_{1.080}$ increases K_f by 41% due to increased thrust forces [17,52].

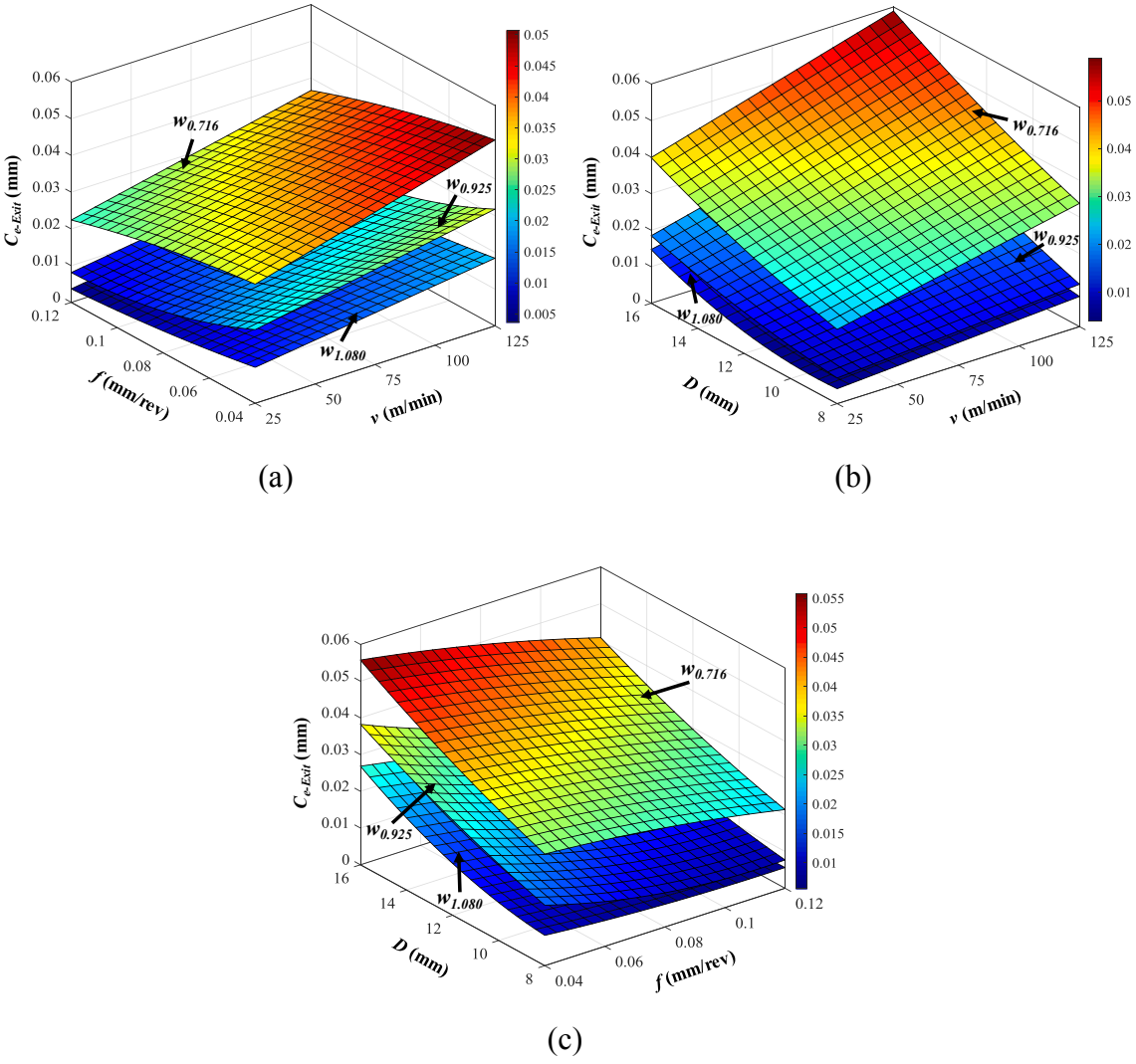

Fig. 10. Response surface plots of (a) v-f, (b) v-D and (c) f-D on Ce-Exit for varying wall thickness.

3.4.4. Cylindricity

CYL increases with increasing cutting speed at all the levels of feeds as seen in Fig. 9a. Increasing feed from $f_{0.04}$ to $f_{0.12}$ increases *CYL* by 40, 77 and 72% for $w_{0.716}$, $w_{0.925}$ and $w_{1.080}$ respectively. Better tool stability at lower feeds results in reduced *CYL* values [53,54]. *CYL* increases with increasing cutting speed and drill diameter (Fig. 9b). Increasing cutting speed form v_{25} to v_{125} increases *CYL* by 29, 24 and 8% for $w_{0.716}$, $w_{0.925}$ and $w_{1.080}$ respectively. At higher cutting speeds the vibration of the cutting tool increases, which leads to the scatting of machine main shaft resulting in higher *CYL* values [55].

Fig. 9c shows the variation of *CYL* with feed and drill diameter. *CYL* increases by 57, 127 and 159% for $w_{0.716}$, $w_{0.925}$ and $w_{1.080}$ respectively for increasing the diameter from D_8 to D_{16}. Increasing drill diameter increases the thrust force generated during the process, which in turn increases the *CYL* values [54]. Increasing GMBs wall thickness decreases the cylindricity of the drill hole significantly i.e. 41% (Fig. 9). It is known that the thermal and dimensional stability of SFs increases with increasing GMBs wall thickness, which subsequently reduces the cylindricity [20,21].

3.4.5. Circularity error at exit

Fig. 10 presents influence of *w*, *v*, *f* and *D* on the circularity error. It is found that increasing the feed decreases the $C_{e\text{-}Exit}$ of the drilled holes (Fig. 10a). Increasing feed from $f_{0.04}$ to $f_{0.12}$ decreases $C_{e\text{-}Exit}$ in the range of 31–61% for varying wall thickness. Increasing feed decreases the work-tool contact time due to increased tool traverse speed. This reduces the rubbing action of tool against the drilled hole wall which in turn decreases circularity error. Increasing feed increases the friction between drill and SF. Nevertheless, frictional heat generated may not be sufficient enough to decrease SF stiffness which results in a quality hole. A similar effect of feed on circularity error in drilling of CFRP is observed in Ref. [29]. Circularity error increases by 32, 78 and 163% for $w_{0.716}$, $w_{0.925}$ and $w_{1.080}$ respectively for increased cutting speed (Fig. 10b). Increasing *v* increases cutting tool rubbing against drilled wall resulting in higher surface distortion leading to higher $C_{e\text{-}Exit}$ values. Also, increasing cutting speed decreases cutting tool stability due to increased chatter vibrations resulting increased circularity errors [56]. $C_{e\text{-}Exit}$ is found to be increasing with increasing feed and drill diameter (Fig. 10c). Increasing drill diameter increases the thrust force

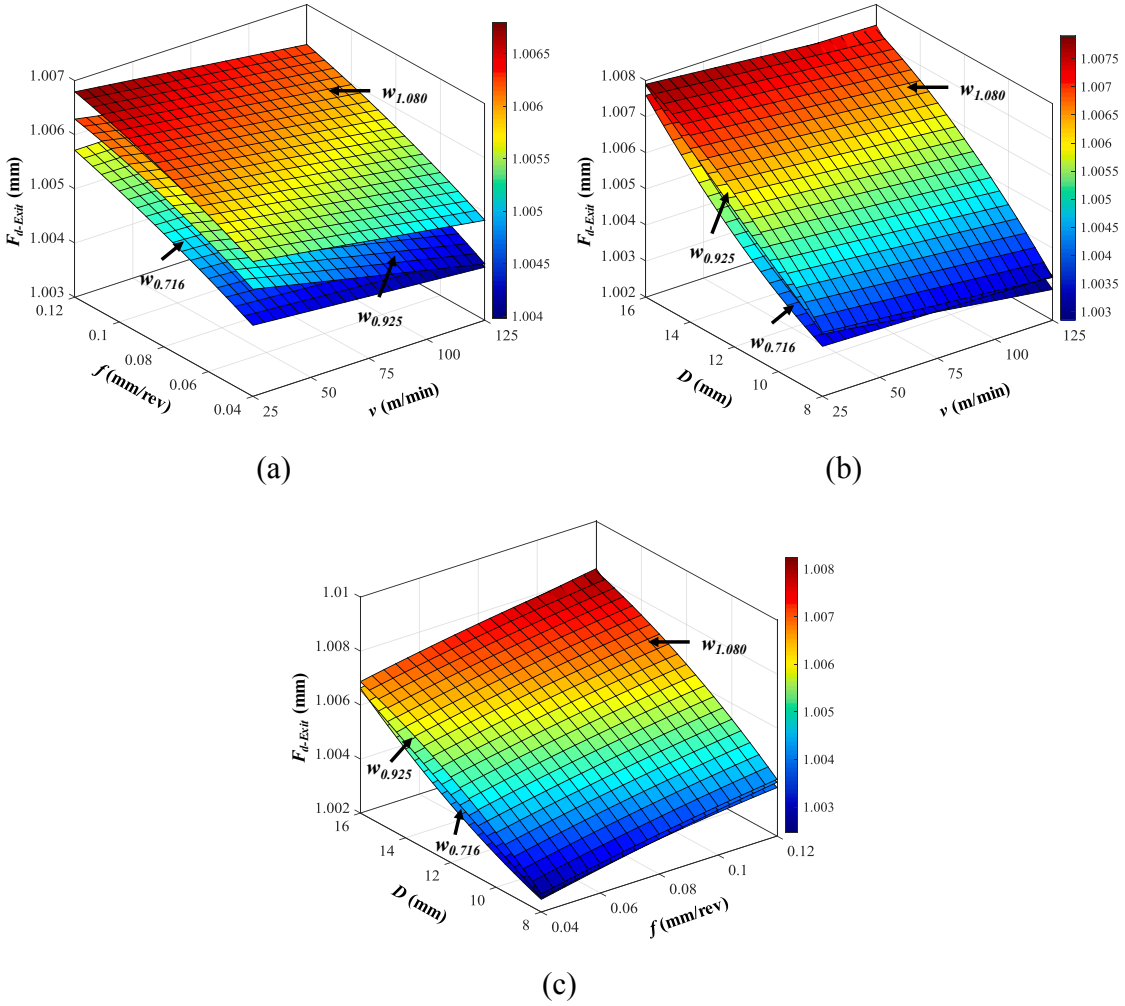

Fig. 11. Response surface plots of (a) v-f, (b) v-D and (c) f-D on Fd-Exit for varying wall thickness.

owing to higher contact area resulting in higher circularity error [22,56]. Increasing GMBs wall thickness decreases the circularity error by 56%. Reinforcing the epoxy matrix with thick-walled GMBs significantly improves the mechanical and thermal properties of syntactic foams resulting in the increased stiffness of syntactic foams which in turn helps to reduce the circularity error of drilled holes [21,57].

3.4.6. Damage factor at exit

Fig. 11a shows the variation of $F_{d\text{-}Exit}$ with cutting speed and feed. It is observed that increasing feed from $f_{0.04}$ to $f_{0.12}$ increases the damage factor by 34, 27 and 24% for $w_{0.716}$, $w_{0.925}$ and $w_{1.080}$ respectively. Increasing f increases F_t due to the increased cutting resistance of syntactic foam leading to higher values of $F_{d\text{-}Exit}$ [27]. Increasing cutting speed increases damage factor for the SF with $w_{1.080}$ GMB while decreasing trend is observed for other SFs (Fig. 11b). $F_{d\text{-}Exit}$ solely depends on the F_t developed during the drilling process [27]. Increasing speed from v_{25} to v_{125} decreases $F_{d\text{-}Exit}$ by 41 and 22% for $w_{0.716}$ and $w_{0.925}$ respectively while it is seen to be increasing by 25% for $w_{1.080}$. SF reinforced with thick-walled GMBs exhibits higher cutting resistance for the advancement of tool into the work material leading to higher thrust forces which results in higher $F_{d\text{-}Exit}$ values. However, delamination factor decreases with increasing cutting speed for $w_{0.716}$ and $w_{0.925}$ due to thermal softening of SF as a result of increased friction between cutting edges and work material [31]. Increasing drill diameter increases the $F_{d\text{-}Exit}$ by 204, 156 and 128% for $w_{0.716}$, $w_{0.925}$ and $w_{1.080}$ respectively (Fig. 11c). With increasing D, F_t increases due to the increased contact area of hole leading to higher $F_{d\text{-}Exit}$ values [22,27]. Increasing GMB wall thickness from $w_{0.716}$ to $w_{1.080}$ increases the $F_{d\text{-}Exit}$ by 40% owing to increased thrust forces. Fig. 12 shows the microscopic image of exit side of the drilled hole. Syntactic foam reinforced with thin-walled GMBs suffers less damage as compared to that with thick-walled GMBs. Increasing GMB wall thickness increases thrust forces which in turn increases the damage on the exit side of the drilled hole.

It is observed from main effect plots (Fig. 5) that the conditions for minimizing all the responses are not same. Lower GMBs wall thickness is desired for reducing F_t, K_f, $F_{d\text{-}Exit}$ whereas thick-walled GMBs are required to minimize R_a, CYL, $C_{e\text{-}Exit}$. Higher cutting speed decreases F_t, K_f, $F_{d\text{-}Exit}$ while lower cutting speed minimizes R_a, CYL, $C_{e\text{-}Exit}$. Lower feed minimizes F_t, CYL, $F_{d\text{-}Exit}$ while higher levels of feed is required to minimize R_a, K_f, $C_{e\text{-}Exit}$. Similarly, all the responses except surface roughness can be minimized by using smaller diameter drills. The trade-off between various process parameters for minimizing the responses

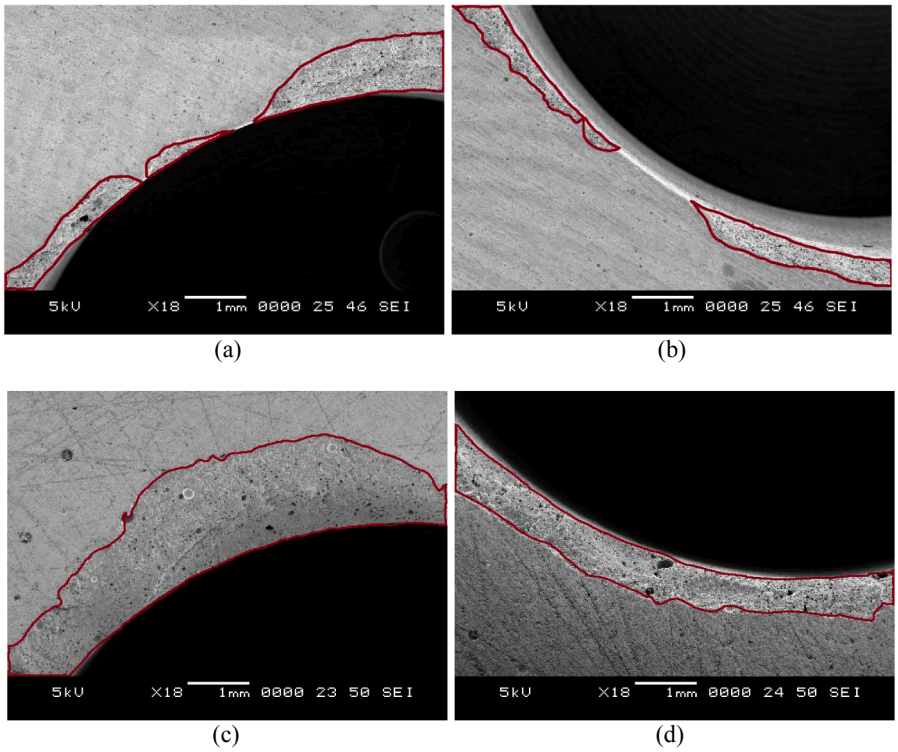

Fig. 12. Microscopic observation of representative (a–b) E200 and (c–d) E350 syntactic foam exit side for damage assessment.

requires multi-response optimization. Hence, in this work, GRA is used for finding a specific combination of process parameters to minimize the responses (F_t, R_a, K_f, CYL, $C_{e\text{-}Exit}$ and $F_{d\text{-}Exit}$) in drilling investigations of GMB reinforced epoxy matrix.

3.5. Grey relation analysis

The first step in GRA is to normalize the experimental data which is also called data pre-processing. In this step measured value of the responses are converted between 0 and 1 for comparison. Since the objective is to find the minimum value of the responses, lower-the-better characteristic of GRA is adopted and is given by [27],

$$Y_e^*(p) = \left(\frac{\max Y_e^o(p) - Y_e^o(p)}{\max Y_e^o(p) - \min Y_e^o(p)} \right) \tag{11}$$

where $e = 1. \ldots m$; $p = 1. \ldots n$

Table 5 presents the normalized data of the measured responses.

In the second step grey relation coefficients are computed using [27],

$$\xi_e(p) = \left(\frac{\Delta_{\min} + \zeta \Delta_{\max}}{\Delta_{oe}(p) + \zeta \Delta_{\max}} \right) \tag{12}$$

$\zeta = 0.5$ [27], is the identification coefficient. Grey relation coefficients of the all measured responses are presented in Table 6.

Finally, grey relation grade is computed by averaging grey relation coefficients which is given by [27],

$$\gamma_e = \frac{1}{n} \sum_{p=1}^{n} \xi_e(p) \tag{13}$$

Table 7 presents the grey relation grades of the measured responses along with the ranks. Highest value (0.741) of grey relation grade is noted to be for $w_{1.080} v_{25} f_{0.12} D_8$ and is the optimized condition for response minimization. By performing drilling at this parameter setting, responses can be effectively minimized to achieve best hole quality.

Furthermore, it is necessary to analyse the effects of process parameters on the machining performance at the optimized condition ($w_{1.080} v_{25} f_{0.12} D_8$). This is performed using the average analysis and results are presented in Table 8. Response table (Table 8) is used to draw grey relation grade graph and is presented in Fig. 13. It is observed from Fig. 13 and Table 8 that the drill diameter is having a significant effect on the drilling performance at the optimized condition followed by cutting speed and wall thickness of GMBs. ANOVA is performed on the grey relation grades to compute the percentage contribution of process parameters at the optimized condition and the results are presented in Table 9. From Table 9 it is clear that the drill diameter has a significant effect on the machining performance followed by the interaction between GMB wall thickness and cutting speed. Thick walled microballoons (SID-350Z having weight saving potential of ~48%) performed better as compared to thin walled ones (SID-200Z). These observations offer guidelines for the industries to produce quality holes in GMB/epoxy syntactic foams used for structural applications.

4. Conclusions

Three types of syntactic foams are prepared using different grades of GMBs (varying wall thickness) in the epoxy matrix at 60 vol%. Fabricated syntactic foams are drilled using CNC vertical machining center with coated tungsten carbide twist drills. FFD based experiments are performed to analyse the effect of process parameters on the

Table 5
Normalized data (Smaller is better).

w	v	f	D	F_t	R_a	K_f	CYL	C_{e-Exit}	F_{d-Exit}
0.716	25	0.04	8	1.000	0.160	0.667	0.688	0.632	0.757
			12	0.800	0.492	0.444	0.646	0.526	0.591
			16	0.600	0.666	0.333	0.521	0.281	0.320
		0.08	8	0.900	0.393	0.833	0.646	0.719	0.728
			12	0.700	0.645	0.778	0.521	0.526	0.524
			16	0.400	0.701	0.667	0.417	0.316	0.223
		0.12	8	0.800	0.413	0.889	0.500	0.772	0.583
			12	0.500	0.646	0.815	0.479	0.684	0.447
			16	0.200	0.874	0.778	0.250	0.509	0.131
	75	0.04	8	1.000	0.160	0.667	0.688	0.561	0.910
			12	0.900	0.414	0.667	0.583	0.421	0.621
			16	0.700	0.654	0.500	0.375	0.070	0.379
		0.08	8	0.900	0.345	0.833	0.625	0.596	0.734
			12	0.700	0.472	0.778	0.438	0.456	0.524
			16	0.500	0.614	0.750	0.313	0.281	0.320
		0.12	8	0.900	0.404	1.000	0.500	0.737	0.704
			12	0.600	0.501	0.889	0.417	0.596	0.524
			16	0.300	0.787	0.833	0.146	0.351	0.175
	125	0.04	8	1.000	0.127	0.667	0.646	0.526	1.000
			12	0.900	0.362	0.667	0.500	0.281	0.743
			16	0.800	0.444	0.667	0.292	0.000	0.534
		0.08	8	1.000	0.193	1.000	0.625	0.596	0.816
			12	0.800	0.395	0.889	0.438	0.351	0.633
			16	0.600	0.554	0.833	0.271	0.228	0.451
		0.12	8	0.900	0.260	1.000	0.479	0.719	0.728
			12	0.700	0.529	0.963	0.313	0.509	0.677
			16	0.500	0.646	0.944	0.000	0.316	0.245
0.925	25	0.04	8	0.900	0.435	0.333	0.938	0.825	0.728
			12	0.700	0.559	0.222	0.854	0.614	0.546
			16	0.600	0.926	0.333	0.583	0.596	0.253
		0.08	8	0.800	0.458	0.667	0.854	0.930	0.644
			12	0.500	0.881	0.556	0.667	0.877	0.398
			16	0.300	0.926	0.583	0.521	0.702	0.188
		0.12	8	0.800	0.680	0.889	0.729	0.982	0.569
			12	0.500	0.911	0.815	0.604	0.895	0.359
			16	0.100	0.929	0.722	0.292	0.789	0.097
	75	0.04	8	0.900	0.378	0.333	0.854	0.754	0.757
			12	0.800	0.505	0.444	0.750	0.561	0.576
			16	0.600	0.687	0.333	0.563	0.421	0.285
		0.08	8	0.800	0.420	0.667	0.813	0.860	0.705
			12	0.600	0.586	0.667	0.604	0.772	0.439
			16	0.400	0.708	0.667	0.375	0.509	0.242
		0.12	8	0.800	0.559	0.889	0.688	0.895	0.654
			12	0.600	0.644	0.889	0.458	0.807	0.435
			16	0.200	0.816	0.778	0.292	0.719	0.141
	125	0.04	8	1.000	0.000	0.667	0.792	0.684	0.864
			12	0.800	0.443	0.444	0.625	0.561	0.575
			16	0.600	0.534	0.333	0.458	0.088	0.401
		0.08	8	0.900	0.231	0.833	0.771	0.825	0.736
			12	0.600	0.523	0.667	0.521	0.649	0.466
			16	0.400	0.657	0.667	0.292	0.456	0.312
		0.12	8	0.800	0.245	0.889	0.604	0.860	0.673
			12	0.600	0.524	0.889	0.458	0.702	0.446
			16	0.200	0.809	0.778	0.208	0.526	0.174
1.080	25	0.04	8	0.900	0.499	0.333	0.938	0.947	0.700
			12	0.700	0.980	0.222	0.896	0.895	0.437
			16	0.400	0.669	0.000	0.688	0.649	0.248
		0.08	8	0.800	0.639	0.667	0.854	0.982	0.629
			12	0.600	1.000	0.667	0.771	0.930	0.393
			16	0.200	0.910	0.500	0.563	0.825	0.161
		0.12	8	0.800	0.715	0.889	0.833	1.000	0.550
			12	0.500	0.946	0.815	0.667	0.965	0.295
			16	0.200	0.918	0.778	0.396	0.860	0.073
	75	0.04	8	0.900	0.453	0.333	1.000	0.877	0.728
			12	0.800	0.751	0.444	0.896	0.807	0.422
			16	0.500	0.531	0.167	0.729	0.596	0.233
		0.08	8	0.800	0.443	0.667	0.938	0.895	0.641
			12	0.500	0.809	0.556	0.854	0.860	0.277
			16	0.100	0.767	0.417	0.583	0.596	0.136
		0.12	8	0.700	0.596	0.778	0.854	0.930	0.567
			12	0.500	0.836	0.815	0.833	0.877	0.277
			16	0.000	0.554	0.667	0.542	0.754	0.087
	125	0.04	8	1.000	0.297	0.667	0.875	0.807	0.636
			12	0.700	0.864	0.222	0.771	0.667	0.340
			16	0.400	0.720	0.000	0.646	0.404	0.155
		0.08	8	0.800	0.002	0.667	0.813	0.877	0.511
			12	0.500	0.780	0.556	0.750	0.754	0.233
			16	0.100	0.841	0.417	0.500	0.509	0.107
		0.12	8	0.700	0.271	0.778	0.813	0.877	0.422
			12	0.400	0.947	0.741	0.646	0.754	0.204
			16	0.000	0.881	0.667	0.375	0.544	0.000

machining performance. Mathematical models developed based on experimental results to predict the responses in the chosen range are validated using ANOVA. Interaction effects among the process parameters on drilling characteristics are analysed using the developed mathematical models. Furthermore, grey relation optimization is carried out to obtain a combination of process parameters to achieve the best hole quality. Conclusions are summarised as:

- Thrust force is found to be increased with higher feed, drill diameter and GMB wall thickness, while it decreases with increasing cutting speed except for syntactic foam with thick-walled GMBs.
- Increasing wall thickness of GMBs increases thrust force by 40% due to the increased cutting resistance of syntactic foam having thick-walled GMBs.
- Surface roughness increases with increasing cutting speed while lowers with higher feed and GMB wall thickness. Increasing drill diameter from D_8 toD_{16}decreases surface roughness of drilled holes whereas an increasing trend beyond D_{12} is observed for thick-walled syntactic foams.
- Surface roughness is found to be decreased by 30% with increasing GMB wall thickness due to the improved thermal stability of syntactic foams.
- Specific cutting coefficient and exit side damage factor depend on the thrust force. Increasing GMB wall thickness and drill diameter increases both K_f and F_{d-Exit}. Increasing wall thickness of GMBs increases K_f and F_{d-Exit} by nearly 40% due to increased thrust forces.
- Cylindricity decreases with increasing GMB wall thickness and seen to be increasing with higher cutting speed, feed and drill diameter. Exit side circularity error is found to be decreasing with increasing GMB wall thickness and feed, whilst it increases with increasing cutting speed and drill diameter.
- Cylindricity and circularity error is found to be decreased by 41 and 56% respectively with increasing GMB wall thickness because of the increased thermal conductivity of foams.
- Grey relation optimization results reveal that performing machining at a combination of higher particle wall thickness and feed, lower cutting speed and drill diameter ($w_{1.080}v_{25}f_{0.12}D_8$) effectively minimizes the responses and helps in obtaining the best quality hole.
- At the optimized condition, drill diameter has a profound effect on the machining performance followed by cutting speed and GMB wall thickness.

Observations and parameters settings explored in this work can guide the industrial practitioners dealing with joining/assembling syntactic foam components for weight sensitive applications.

Table 6
Grey relation coefficients.

w	v	f	D	F_t	R_a	K_f	CYL	C_{e-Exit}	F_{d-Exit}
0.716	25	0.04	8	1.000	0.373	0.600	0.615	0.576	0.673
			12	0.714	0.496	0.474	0.585	0.514	0.550
			16	0.556	0.600	0.429	0.511	0.410	0.424
		0.08	8	0.833	0.452	0.750	0.585	0.640	0.648
			12	0.625	0.585	0.692	0.511	0.514	0.512
			16	0.455	0.626	0.600	0.462	0.422	0.392
		0.12	8	0.714	0.460	0.818	0.500	0.687	0.545
			12	0.500	0.586	0.730	0.490	0.613	0.475
			16	0.385	0.799	0.692	0.400	0.504	0.365
	75	0.04	8	1.000	0.373	0.600	0.615	0.533	0.848
			12	0.833	0.461	0.600	0.545	0.463	0.569
			16	0.625	0.591	0.500	0.444	0.350	0.446
		0.08	8	0.833	0.433	0.750	0.571	0.553	0.653
			12	0.625	0.486	0.692	0.471	0.479	0.512
			16	0.500	0.565	0.667	0.421	0.410	0.424
		0.12	8	0.833	0.456	1.000	0.500	0.655	0.628
			12	0.556	0.500	0.818	0.462	0.553	0.512
			16	0.417	0.701	0.750	0.369	0.435	0.377
	125	0.04	8	1.000	0.364	0.600	0.585	0.514	1.000
			12	0.833	0.439	0.600	0.500	0.410	0.660
			16	0.714	0.474	0.600	0.414	0.333	0.518
		0.08	8	1.000	0.382	1.000	0.571	0.553	0.730
			12	0.714	0.452	0.818	0.471	0.435	0.577
			16	0.556	0.529	0.750	0.407	0.393	0.477
		0.12	8	0.833	0.403	1.000	0.490	0.640	0.648
			12	0.625	0.515	0.931	0.421	0.504	0.607
			16	0.500	0.585	0.900	0.333	0.422	0.398
0.925	25	0.04	8	0.833	0.470	0.429	0.889	0.740	0.648
			12	0.625	0.531	0.391	0.774	0.564	0.524
			16	0.556	0.872	0.429	0.545	0.553	0.401
		0.08	8	0.714	0.480	0.600	0.774	0.877	0.584
			12	0.500	0.808	0.529	0.600	0.803	0.454
			16	0.417	0.872	0.545	0.511	0.626	0.381
		0.12	8	0.714	0.610	0.818	0.649	0.966	0.537
			12	0.500	0.849	0.730	0.558	0.826	0.438
			16	0.357	0.876	0.643	0.414	0.704	0.356
	75	0.04	8	0.833	0.446	0.429	0.774	0.671	0.673
			12	0.714	0.503	0.474	0.667	0.533	0.541
			16	0.556	0.615	0.429	0.533	0.463	0.412
		0.08	8	0.714	0.463	0.600	0.727	0.781	0.629
			12	0.556	0.547	0.600	0.558	0.687	0.471
			16	0.455	0.631	0.600	0.444	0.504	0.398
		0.12	8	0.714	0.531	0.818	0.615	0.826	0.591
			12	0.556	0.584	0.818	0.480	0.722	0.469
			16	0.385	0.731	0.692	0.414	0.640	0.368
	125	0.04	8	1.000	0.333	0.600	0.706	0.613	0.787
			12	0.714	0.473	0.474	0.571	0.533	0.541
			16	0.556	0.517	0.429	0.480	0.354	0.455
		0.08	8	0.833	0.394	0.750	0.686	0.740	0.655
			12	0.556	0.512	0.600	0.511	0.588	0.484
			16	0.455	0.593	0.600	0.414	0.479	0.421
		0.12	8	0.714	0.398	0.818	0.558	0.781	0.605
			12	0.556	0.512	0.818	0.480	0.626	0.474
			16	0.385	0.724	0.692	0.387	0.514	0.377
1.080	25	0.04	8	0.833	0.499	0.429	0.889	0.905	0.625
			12	0.625	0.961	0.391	0.828	0.826	0.470
			16	0.455	0.602	0.333	0.615	0.588	0.399
		0.08	8	0.714	0.581	0.600	0.774	0.966	0.574
			12	0.556	1.000	0.600	0.686	0.877	0.452
			16	0.385	0.847	0.500	0.533	0.740	0.373
		0.12	8	0.714	0.637	0.818	0.750	1.000	0.526
			12	0.500	0.902	0.730	0.600	0.934	0.415
			16	0.385	0.859	0.692	0.453	0.781	0.350
	75	0.04	8	0.833	0.478	0.429	1.000	0.803	0.648
			12	0.714	0.667	0.474	0.828	0.722	0.464
			16	0.500	0.516	0.375	0.649	0.553	0.395
		0.08	8	0.714	0.473	0.600	0.889	0.826	0.582
			12	0.500	0.724	0.529	0.774	0.781	0.409
			16	0.357	0.682	0.462	0.545	0.553	0.367
		0.12	8	0.625	0.553	0.692	0.774	0.877	0.536
			12	0.500	0.753	0.730	0.750	0.803	0.409
			16	0.333	0.528	0.600	0.522	0.671	0.354
	125	0.04	8	1.000	0.416	0.600	0.800	0.722	0.579
			12	0.625	0.786	0.391	0.686	0.600	0.431
			16	0.455	0.641	0.333	0.585	0.456	0.372
		0.08	8	0.714	0.334	0.600	0.727	0.803	0.506
			12	0.500	0.695	0.529	0.667	0.671	0.395
			16	0.357	0.759	0.462	0.500	0.504	0.359
		0.12	8	0.625	0.407	0.692	0.727	0.803	0.464
			12	0.455	0.904	0.659	0.585	0.671	0.386
			16	0.333	0.808	0.600	0.444	0.523	0.333

Table 7
Grey relation grade and rank.

v	f	D	$w_{0.716}$		$w_{0.925}$		$w_{1.080}$	
			γ_e	Rank	γ_e	Rank	γ_e	Rank
25	0.04	8	0.640	28	0.668	20	0.697	6
		12	0.556	56	0.568	49	0.684	9
		16	0.488	79	0.559	53	0.499	71
	0.08	8	0.651	24	0.672	18	0.702	4
		12	0.573	46	0.616	34	0.695	7
		16	0.493	76	0.559	54	0.563	52
	0.12	8	0.621	31	0.716	2	0.741	1
		12	0.565	51	0.650	25	0.680	12
		16	0.524	61	0.558	55	0.587	39
75	0.04	8	0.661	21	0.638	29	0.698	5
		12	0.579	41	0.572	47	0.645	27
		16	0.493	77	0.501	70	0.498	72
	0.08	8	0.632	30	0.652	23	0.681	11
		12	0.544	58	0.570	48	0.619	33
		16	0.498	73	0.505	68	0.494	74
	0.12	8	0.679	13	0.683	10	0.676	16
		12	0.567	50	0.605	37	0.657	22
		16	0.508	66	0.538	60	0.501	69
125	0.04	8	0.677	14	0.673	17	0.686	8
		12	0.574	45	0.551	57	0.586	40
		16	0.509	65	0.465	81	0.474	80
	0.08	8	0.706	3	0.676	15	0.614	35
		12	0.578	42	0.542	59	0.576	44
		16	0.518	63	0.494	75	0.490	78
	0.12	8	0.669	19	0.646	26	0.620	32
		12	0.601	38	0.578	43	0.610	36
		16	0.523	62	0.513	64	0.507	67

Table 8
Response table for grey relation grade.

Level	Mean GRG			
	w	v	f	D
1	0.57879	0.611966	0.58657	0.66941
2	0.59137	0.588715	0.589384	0.59777
3	0.61035	0.579827	0.604553	0.51332
Delta	0.03156	0.032139	0.017983	0.15609
Rank	3	2	4	1

Acknowledgment

Authors thank the Mechanical Engineering Department at NITK for providing facilities and support. The views expressed in this article are those of authors, not of funding agencies.

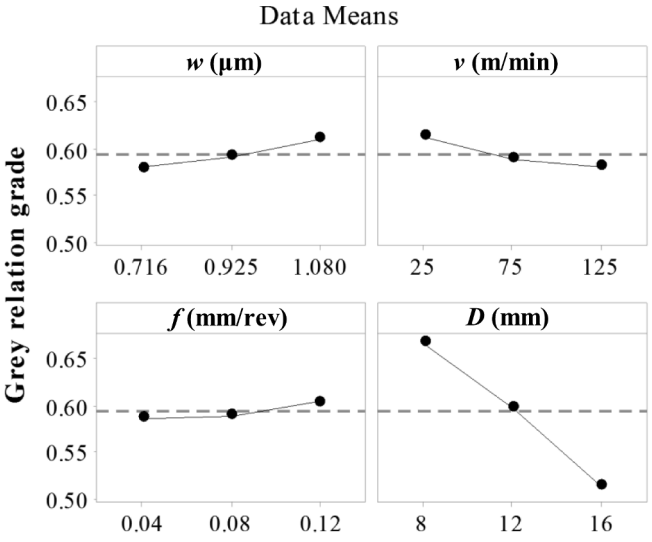

Fig. 13. Grey relation grade graph.

Table 9
ANOVA for grey relation grade.

Source	DF	Adj SS	Adj MS	F-Value	P-Value	% Contribution
w	2	0.014	0.007	19.86	0.00	3.19
v	2	0.015	0.007	21.66	0.00	3.48
f	2	0.005	0.003	7.36	0.00	1.18
D	2	0.330	0.165	480.16	0.00	77.15
*w*v*	4	0.026	0.006	18.70	0.00	6.01
*w*f*	4	0.002	0.000	1.15	0.35	0.37
*w*D*	4	0.013	0.003	9.51	0.00	3.05
*v*f*	4	0.003	0.001	1.85	0.14	0.59
*v*D*	4	0.002	0.001	1.73	0.16	0.55
*f*D*	4	0.002	0.001	1.72	0.16	0.55
Error	48	0.016	0.000			
Total	80	0.427				

Data Availability

The raw/processed data required to reproduce these findings cannot be shared at this time as the data also forms part of an ongoing study.

References

[1] Syntactic FA. Syntactic polymer foams. Berlin, Heidelberg: Springer Berlin Heidelberg; 1986.
[2] Gupta N, Woldesenbet E. Microballoon wall thickness effects on properties of syntactic foams. J Cell Plast 2004;40(6):461–80.
[3] Gupta N, Zeltmann SE, Shunmugasamy VC, Pinisetty D. Applications of polymer matrix syntactic foams. JOM 2014;66(2):245–54.
[4] Gupta N, Pinisetty D, Shunmugasamy VC. Reinforced polymer matrix syntactic foams: effect of nano and micro-scale reinforcement. Springer Science & Business Media; 2013.
[5] Jayavardhan ML, Doddamani M. Quasi-static compressive response of compression molded glass microballoon/HDPE syntactic foam. Compos B Eng 2018;149:165–77.
[6] Garcia CD, Shahapurkar K, Doddamani M, Kumar GCM, Prabhakar P. Effect of arctic environment on flexural behavior of fly ash cenosphere reinforced epoxy syntactic foams. Compos B Eng 2018;151:265–73.
[7] Shahapurkar K, Garcia CD, Doddamani M, Mohan Kumar GC, Prabhakar P. Compressive behavior of cenosphere/epoxy syntactic foams in arctic conditions. Compos B Eng 2018;135:253–62.
[8] Singh AK, Patil B, Hoffmann N, Saltonstall B, Doddamani M, Gupta N. Additive manufacturing of syntactic foams: Part 1: development, properties, and recycling potential of filaments. JOM 2018;70(3):303–9.
[9] Singh AK, Saltonstall B, Patil B, Hoffmann N, Doddamani M, Gupta N. Additive manufacturing of syntactic foams: Part 2: specimen printing and mechanical property characterization. JOM 2018;70(3):310–4.
[10] Jayavardhan ML, Bharath Kumar BR, Doddamani M, Singh AK, Zeltmann SE, Gupta N. Development of glass microballoon/HDPE syntactic foams by compression molding. Compos B Eng 2017;130(Supplement C):119–31.
[11] Mathapati M, Ramesh MR, Doddamani M. High temperature erosion behavior of plasma sprayed NiCrAlY/WC-Co/cenosphere coating. Surf Coat Technol 2017;325:98–106.
[12] Doddamani M, Kulkarni S. Dynamic response of fly ash reinforced functionally graded rubber composite sandwiches-a Taguchi approach. Int J Eng Sci Technol 2011;3(1):17.
[13] Pinisetty D, Shunmugasamy VC, Gupta N. Hollow glass microspheres in thermosets-epoxy syntactic foams. Hollow glass microspheres for plastics, elastomers, and adhesives compounds. Elsevier Inc.; 2015.
[14] Wouterson EM, Boey FYC, Hu X, Wong S-C. Specific properties and fracture toughness of syntactic foam: effect of foam microstructures. Compos Sci Technol 2005;65(11):1840–50.
[15] Swetha C, Kumar R. Quasi-static uni-axial compression behaviour of hollow glass microspheres/epoxy based syntactic foams. Mater Des 2011;32(8):4152–63.
[16] Kim HS, Plubrai P. Manufacturing and failure mechanisms of syntactic foam under compression. Compos A Appl Sci Manuf 2004;35(9):1009–15.
[17] Gupta N, Priya S, Islam R, Ricci W. Characterization of mechanical and electrical properties of epoxy-glass microballoon syntactic composites. Ferroelectrics 2006;345(1):1–12.
[18] Kishore R Shankar, Sankaran S. Gradient syntactic foams: tensile strength, modulus and fractographic features. Mater Sci Eng, A 2005;412(1):153–8.
[19] Gupta N, Nagorny R. Tensile properties of glass microballoon-epoxy resin syntactic foams. J Appl Polym Sci 2006;102(2):1254–61.
[20] Park S-J, Jin F-L, Lee C. Preparation and physical properties of hollow glass microspheres-reinforced epoxy matrix resins. Mater Sci Eng, A 2005;402(1):335–40.
[21] Zeltmann SE, Chen B, Gupta N. Thermal expansion and dynamic mechanical analysis of epoxy matrix–borosilicate glass hollow particle syntactic foams. J Cell Plast 2018;54(3):463–81.
[22] El-Sonbaty I, Khashaba U, Machaly T. Factors affecting the machinability of GFR/epoxy composites. Compos Struct 2004;63(3):329–38.
[23] Gaitonde V, Karnik S, Rubio JC, Abrão A, Correia AE, Davim JP. Surface roughness analysis in high-speed drilling of unreinforced and reinforced polyamides. J Compos Mater 2012;46(21):2659–73.
[24] Rubio JCC, da Silva LJ, de Oliveira Leite W, Panzera TH, Ribeiro Filho SLM, Davim JP. Investigations on the drilling process of unreinforced and reinforced polyamides using Taguchi method. Compos B Eng 2013;55:338–44.
[25] Liu Z, Xu J, Han S, Chen M. A coupling method of response surfaces (CRSM) for cutting parameters optimization in machining titanium alloy under minimum quantity lubrication (MQL) condition. Int J Precis Eng Manuf 2013;14(5):693–702.
[26] Palanikumar K, Latha B, Senthilkumar VS, Davim JP. Analysis on drilling of glass fiber-reinforced polymer (GFRP) composites using grey relational analysis. Mater Manuf Processes 2012;27(3):297–305.
[27] Palanikumar K. Experimental investigation and optimisation in drilling of GFRP composites. Measurement 2011;44(10):2138–48.
[28] Basavarajappa S, Venkatesh A, Gaitonde V, Karnik S. Experimental investigations on some aspects of machinability in drilling of glass epoxy polymer composites. J Thermoplast Compos Mater 2012;25(3):363–87.
[29] Krishnaraj V, Prabukarthi A, Ramanathan A, Elanghovan N, Senthil Kumar M, Zitoune R, et al. Optimization of machining parameters at high speed drilling of carbon fiber reinforced plastic (CFRP) laminates. Compos B Eng 2012;43(4):1791–9.
[30] Hrechuk A, Bushlya V, Ståhl J-E. Hole-quality evaluation in drilling fiber-reinforced composites. Compos Struct 2018;204:378–87.
[31] Xu J, An Q, Cai X, Chen M. Drilling machinability evaluation on new developed high-strength T800S/250F CFRP laminates. Int J Precis Eng Manuf 2013;14(10):1687–96.
[32] Xu J, Li C, Mi S, An Q, Chen M. Study of drilling-induced defects for CFRP composites using new criteria. Compos Struct 2018;201:1076–87.
[33] Xu J, El Mansori M. Experimental study on drilling mechanisms and strategies of hybrid CFRP/Ti stacks. Compos Struct 2016;157:461–82.
[34] Ameur M, Habak M, Kenane M, Aouici H, Cheikh M. Machinability analysis of dry drilling of carbon/epoxy composites: cases of exit delamination and cylindricity error. Int J Adv Manuf Technol 2017;88(9–12):2557–71.
[35] Saoudi J, Zitoune R, Mezlini S, Gururaja S, Seitier P. Critical thrust force predictions during drilling: analytical modeling and X-ray tomography quantification. Compos Struct 2016;153:886–94.
[36] Sorrentino L, Turchetta S, Bellini C. In process monitoring of cutting temperature during the drilling of FRP laminate. Compos Struct 2017;168:549–61.
[37] Merino-Perez JL, Royer R, Merson E, Lockwood A, Ayvar-Soberanis S, Marshall MB. Influence of workpiece constituents and cutting speed on the cutting forces developed in the conventional drilling of CFRP composites. Compos Struct 2016;140:621–9.
[38] Ashrith HS, Doddamani M, Gaitonde V, Gupta N. Hole quality assessment in drilling of glass microballoon/epoxy syntactic foams. JOM 2018;70(7):1289–94.
[39] Gaitonde V, Karnik S, Mata F, Davim JP. Study on some aspects of machinability in unreinforced and reinforced polyamides. J Compos Mater 2009;43(7):725–39.
[40] Palanikumar K, Karthikeyan R. Assessment of factors influencing surface roughness on the machining of Al/SiC particulate composites. Mater Des 2007;28(5):1584–91.
[41] Karnik S, Gaitonde V. Development of artificial neural network models to study the effect of process parameters on burr size in drilling. Int J Adv Manuf Technol 2008;39(5–6):439–53.
[42] Abrão AM, Faria PE, Rubio JCC, Reis P, Davim JP. Drilling of fiber reinforced plastics: a review. J Mater Process Technol 2007;186(1):1–7.
[43] Montgomery D. Design and analysis of experiments. New York: John Wiley; 2003.
[44] Sorrentino L, Turchetta S, Bellini C. A new method to reduce delaminations during drilling of FRP laminates by feed rate control. Compos Struct 2018;186:154–64.
[45] Davim JP, Rubio JC, Abrao AM. A novel approach based on digital image analysis to

evaluate the delamination factor after drilling composite laminates. Compos Sci Technol 2007;67(9):1939–45.
[46] Manakari V, Parande G, Doddamani M, Gaitonde VN, Siddhalingeshwar IG, Kishore VC Shunmugasamy, et al. Dry sliding wear of epoxy/cenosphere syntactic foams. Tribol Int 2015;92(Suppl. C):425–38.
[47] Davim JP, Gaitonde V, Karnik S. An investigative study of delamination in drilling of medium density fibreboard (MDF) using response surface models. Int J Adv Manuf Technol 2008;37(1):49–57.
[48] Karnik S, Gaitonde V, Rubio JC, Correia AE, Abrão A, Davim JP. Delamination analysis in high speed drilling of carbon fiber reinforced plastics (CFRP) using artificial neural network model. Mater Des 2008;29(9):1768–76.
[49] Zitoune R, Krishnaraj V, Almabouacif BS, Collombet F, Sima M, Jolin A. Influence of machining parameters and new nano-coated tool on drilling performance of CFRP/Aluminium sandwich. Compos B Eng 2012;43(3):1480–8.
[50] Khashaba U, El-Sonbaty I, Selmy A, Megahed A. Machinability analysis in drilling woven GFR/epoxy composites: Part I-effect of machining parameters. Compos A Appl Sci Manuf 2010;41(3):391–400.
[51] Davim JP, Reis P, Lapa VT, António CC. Machinability study on polyetheretherketone (PEEK) unreinforced and reinforced (GF30) for applications in structural components. Compos Struct 2003;62(1):67–73.
[52] Gaitonde V, Karnik S, Mata F, Davim JP. Modeling and analysis of machinability characteristics in PA6 and PA66 GF30 polyamides through artificial neural network. J Thermoplast Compos Mater 2010;23(3):313–36.
[53] Sultan AZ, Sharif S, Kurniawan D. Effect of machining parameters on tool wear and hole quality of AISI 316L stainless steel in conventional drilling. Procedia Manuf 2015;2:202–7.
[54] Gowda BU, Ravindra H, Jain SP, Raj MN, Prakesh GN, Ugrasen G. Comparative study of surface roughness and cylindricity of aluminium silicon nitride material using MRA GMDH & pattern recognition technique in drilling. Procedia Mater Sci 2014;6:1770–9.
[55] Kurt M, Kaynak Y, Bagci E. Evaluation of drilled hole quality in Al 2024 alloy. Int J Adv Manuf Technol 2008;37(11):1051–60.
[56] Giasin K, Ayvar-Soberanis S. An Investigation of burrs, chip formation, hole size, circularity and delamination during drilling operation of GLARE using ANOVA. Compos Struct 2017;159:745–60.
[57] Gaitonde V, Karnik S, Rubio JCC, Leite WdO, Davim J. Experimental studies on hole quality and machinability characteristics in drilling of unreinforced and reinforced polyamides. J Compos Mater 2014;48(1):21–36.